

# BAYESIAN INVERSION WITH $\alpha$ -STABLE PRIORS

JARKKO SUURONEN, TOMAS SOTO, NEIL K. CHADA, AND LASSI ROININEN

ABSTRACT. We propose to use Lévy  $\alpha$ -stable distributions for constructing priors for Bayesian inverse problems. The construction is based on Markov fields with stable-distributed increments. Special cases include the Cauchy and Gaussian distributions, with stability indices  $\alpha = 1$ , and  $\alpha = 2$ , respectively. Our target is to show that these priors provide a rich class of priors for modelling rough features. The main technical issue is that the  $\alpha$ -stable probability density functions do not have closed-form expressions in general, and this limits their applicability. For practical purposes, we need to approximate probability density functions through numerical integration or series expansions. Current available approximation methods are either too time-consuming or do not function within the range of stability and radius arguments needed in Bayesian inversion. To address the issue, we propose a new hybrid approximation method for symmetric univariate and bivariate  $\alpha$ -stable distributions, which is both fast to evaluate, and accurate enough from a practical viewpoint. Then we use approximation method in the numerical implementation of  $\alpha$ -stable random field priors. We demonstrate the applicability of the constructed priors on selected Bayesian inverse problems which include the deconvolution problem, and the inversion of a function governed by an elliptic partial differential equation. We also demonstrate hierarchical  $\alpha$ -stable priors in the one-dimensional deconvolution problem. We employ maximum-a-posterior-based estimation at all the numerical examples. To that end, we exploit the limited-memory BFGS and its bounded variant for the estimator.

## 1. INTRODUCTION

Inverse problems is the mathematical theory and practical interpretation of noise-perturbed indirect observations. Bayesian statistical inversion is the effort to formulate real-world inverse problems as Bayesian statistical estimation problems [56, 28]. Bayesian inverse problems can be found in medical and subsurface imaging, industrial applications, and near-space remote sensing. The objective, for example in industrial tomography, is to detect different materials, which may have isotropic, anisotropic, or inhomogeneous features. This means that we typically aim at reconstructing a hidden substance from indirect noise-perturbed measurements. Inhomogeneities include, for example, material interfaces and rough features, and these are the main topics of this paper.

Inverse problems are often formulated through a noise-perturbed measurement equation

$$(1.1) \quad \mathbf{y} = \mathcal{G}(u) + \boldsymbol{\eta}, \quad \boldsymbol{\eta} \sim \mathcal{N}(\mathbf{0}, \mathbf{C}),$$

where  $\mathbf{y} \in \mathbb{R}^M$  are noisy finite-dimensional measurements,  $\mathcal{G}$  is a linear or non-linear mapping from some function space to  $\mathbb{R}^M$ ,  $u \in \mathbb{R}^d$  is the unknown with typically  $d = 1, 2, 3$ , and  $\boldsymbol{\eta}$  is noise, which we assume to be Gaussian. Our aim is to estimate  $u$  given one realisation of  $\mathbf{y}$ .

---

2020 *Mathematics Subject Classification.* 94A12, 86A22, 60G35, 62M99.

*Key words and phrases.* Inverse problems,  $\alpha$ -stable processes, non-Gaussian priors, error bound, deconvolution.

Inverse problems methods can be roughly divided to deterministic and statistical methods. In statistical framework, we model  $\mathbf{y}, u, \boldsymbol{\eta}$  as random objects [28]. For practical computations, we discretize the unknown  $U$ , and denote it by  $\mathbf{u}$ . Then the solution, within Bayesian inverse problems framework, can be represented through probability distributions via Bayes theorem, that is, the posterior distribution

$$\pi(\mathbf{u} | \mathbf{y}) = \frac{\pi(\mathbf{y} | \mathbf{u})\pi(\mathbf{u})}{\pi(\mathbf{y})} \propto \pi(\mathbf{y} | \mathbf{u})\pi(\mathbf{u}),$$

where  $\pi(\mathbf{y} | \mathbf{u})$  is the likelihood, and  $\pi(\mathbf{u})$  is the prior distribution of the unknown. We omit the normalization constant  $\pi(\mathbf{y})$ , and from hereon we simply use unnormalized posterior distribution.

The choice of the prior  $\pi(\mathbf{u})$  is practically the only tuneable object in inversion. The traditional choices in inverse problems are Gaussian and total variation priors for smoothing and edge-preserving inversion, respectively [28, 50, 48, 33]. In this paper, we build upon the research line starting from the observation that total variation priors do not provide invariant estimators under mesh refinement [33]. The solution to this problem was proposed through Besov priors on wavelet basis [32]. In our previous papers [55, 54], we have proposed Cauchy difference priors as alternatives to Besov priors. Here, we extend the study from Cauchy priors to  $\alpha$ -stable priors, of which the Cauchy priors are special cases with  $\alpha = 1$ , and Gaussian priors are similarly special cases with  $\alpha = 2$ .

In order to leverage  $\alpha$ -stable laws for Bayesian inverse problems, we need approximations of  $\alpha$ -stable probability densities evaluated very fast with reasonable precision [46, 45]. Our particular interest is to implement and use discretized  $\alpha$ -stable random fields in Bayesian continuous-parameter estimation.

We note that traditionally, stable distributions have been employed in financial applications, like modeling of asset time series [7]. They have also been applied in biomedical engineering [1], remote sensing [37], statistical analysis of network traffic [24], and digital signal processing [42], some to mention. Here extend the usage to inverse problems.

**1.1. Contributions.** Our objective is to implement numerical approximations of symmetric  $\alpha$ -stable priors for Bayesian inverse problems, which requires evaluating the univariate or multivariate probability density functions of  $\alpha$ -stable random variables. The symmetric  $\alpha$ -stable probability density functions do not have elementary function expressions, except for the two special cases of Gaussian and Cauchy distributions, so the evaluation requires incorporation of an appropriate approximation method [45, 51].

A straightforward approximation is to evaluate the inverse Fourier transform of the characteristic function of the  $\alpha$ -stable distribution. In fact, the  $\alpha$ -stable distributions are often treated and even defined through their characteristic functions. The inverse Fourier transform can be approximated with an adaptive numerical quadrature integration, or with the help of a discrete Fourier transform [44]. The drawback of the numerical integration of the inverse Fourier transform is the cumbersome integrand, which decays slowly when  $\alpha$  is small, and oscillates considerably when the argument  $r$  of the transform is large [44, 3].

The discrete Fourier transform method [53] exploits the low computational complexity of the Fast Fourier Transform Fourier transform, but requires interpolation to evaluate the density at outside the grid [38]. Additionally, there is an alternative integral representation formula for the univariate  $\alpha$ -stable probability density function [46], which does not involve improper integrals with oscillatory integrands, but which cannot be used when  $\alpha$  is close to 1.

The density functions of  $\alpha$ -stable distributions can also be approximated using series expansions [57]. Some of the existing series expansions converge to the true probability density function pointwise for any  $r > 0$ , while the others are asymptotic for either  $r \rightarrow 0^+$  or  $r \rightarrow \infty$  [44, 45]. The latter are particularly useful for approximating the tails of the probability density functions, that may be difficult for the methods based on numerical integration.

Unfortunately, none of the existing  $\alpha$ -stable density function approximation methods are optimal for our needs because they are either computationally too heavy to evaluate within Bayesian inversion, or not applicable for a wide range of values of  $r$  and stability indices  $\alpha$ . For this reason, we introduce a fast hybrid method to approximate the  $\alpha$ -stable laws that uses both bicubic spline interpolations at pre-computed probability density grids, as well as asymptotic series approximations. We also establish error bounds for the method. We demonstrate various  $\alpha$ -stable priors on a range of Bayesian inverse problems. These include deconvolution problems in one- and two-dimensional grids. Finally, we illustrate nonlinear Bayesian inversion governed by an elliptic PDE through  $\alpha$ -stable priors. In the numerical examples, we resort to maximum a posteriori (MAP) estimators:

$$(1.2) \quad \mathbf{u}_{\text{MAP}} := \arg \max_{\mathbf{u}} \pi(\mathbf{u} \mid \mathbf{y}).$$

**1.2. Outline.** This paper is organized as follows: In Section 2, we provide the necessary background material required for the paper as an introduction into  $\alpha$ -stable priors. This will lead onto Section 3, where we briefly review the existing methods and our hybrid method for approximating  $\alpha$ -stable probability density functions, and provide error bounds related to our method. Numerical experiments with the  $\alpha$ -stable priors are provided in Section 4, where we test our priors on the example problems. A summary of our findings and future work are provided in Section 5. Derivations of the error bounds are provided in the Appendix.

## 2. MODELS

In this section we review and discuss the necessary prior forms based on  $\alpha$ -stable distributions. We also present some basic properties, and then present the multivariate setting and how they can be defined.

**2.1. Stable distributions.** A random variable  $W$  corresponding to a symmetric *stable* distribution, also known as  $\alpha$ -*stable* and *Lévy  $\alpha$ -stable* distribution, can be characterized in terms of a *stability index*  $\alpha \in (0, 2]$  (sometimes also called the *tail index* or the *characteristic exponent*), and a scale parameter  $\sigma > 0$ , in the sense that its characteristic function is given by

$$(2.1) \quad \mathbb{E}[\exp(i\theta W)] = \exp(-(\sigma|\theta|)^\alpha), \quad \theta \in \mathbb{R},$$

in which case we write

$$W \sim \mathcal{S}_\alpha(\sigma).$$

The parameter  $\alpha$  is called the stability index because if  $W_1$  and  $W_2$  are two independent copies of  $W$  and  $A, B > 0$ , then

$$(2.2) \quad AW_1 + BW_2 \stackrel{d}{=} CW,$$

with

$$C^\alpha = A^\alpha + B^\alpha.$$

Hence, the symmetric  $\alpha$ -stable distributions are a family of continuous probability distributions that are infinitely divisible, and closed under convolution. The monograph [51] is the standard reference for stable distributions, including the wide class of non-symmetric stable distributions which we do not consider here.

It is immediate from (2.1) that for  $\alpha = 2$ ,  $W$  is normally distributed (with zero mean and variance  $2\sigma^2$ ), and that for  $\alpha = 1$ , it has a Cauchy distribution (with zero median and scale parameter being  $\sigma$ ). Besides these two special cases of  $\alpha$ -stable laws, there are no known closed-form expressions based on elementary function for the density functions of symmetric stable distributions (the other special cases where closed-form expressions are known consist of non-symmetric distributions, such as the univariate Holtsmark distribution).

For  $\alpha < 2$ , it holds that  $\mathbb{E}[|W|^\alpha] = \infty$ , which means that in general an  $\alpha$ -stable distribution has infinite variance, and for  $\alpha \leq 1$  its mean is not well-defined either. However, it does hold that  $\mathbb{E}[|W|^\lambda] < \infty$  for all  $\lambda \in (0, \alpha)$ .

Multivariate stable distributions can be defined in a similar but more complicated manner, with a *spectral measure*  $\Lambda$  in place of the scale parameter  $\sigma$ ; see [51, Chapter 2]. For our purposes it suffices to recall the definition of *spherically contoured stable distributions*: a random vector  $\mathbf{W} =: (W_1, W_2, \dots, W_d)$  on  $\mathbb{R}^d$  is said to have an spherically contoured stable distribution if its characteristic function is given by

$$\mathbb{E}\left[\exp\left(i \sum_{j=1}^d \theta_j W_j\right)\right] = \exp(-(\sigma|\theta|)^\alpha), \quad \theta \in \mathbb{R}^d,$$

where  $\alpha \in (0, 2]$  is again a stability index,  $\sigma > 0$  is a scale parameter and  $|\cdot|$  stands for the standard  $\ell^2$ -based Euclidean norm on  $\mathbb{R}^d$ . We refer to [45] for a treatment of such distributions.

**2.2.  $\alpha$ -stable priors.** A stochastic process  $(W_t)_{t \geq 0}$  is a symmetric  $\alpha$ -stable process if  $\sum_{j=1}^n a_j W_{t_j}$  is a symmetric  $\alpha$ -stable random variable for all finite  $\{t_1, \dots, t_n\} \subset [0, \infty)$  and  $\{a_1, \dots, a_n\} \subset \mathbb{R}$ . We refer to [51, Chapter 3] for the existence and construction of a wide variety of such processes. The process is called  $\alpha$ -stable field, if the previous definition is satisfied for the multivariate case  $\{t_1, \dots, t_n\} \subset \mathbb{R}^K$ .

In particular, we aim to apply discretized priors corresponding to a *Lévy  $\alpha$ -stable motion*, which we take to mean an  $\alpha$ -stable process  $(W_t)_{t \geq 0}$  with some given initial distribution  $W_0 \sim \mu$  and independent increments that satisfies

$$W_t - W_s \sim \mathcal{S}_\alpha(|t - s|^{1/\alpha}) \quad \text{for all } s, t \in [0, \infty), t \neq s.$$

For  $\alpha < 2$ , the Lévy  $\alpha$ -stable motion generally does not have continuous sample paths. However, by [52, Theorem 11.1], there exists a version of this process with càdlàg paths satisfying

$$(2.3) \quad \mathbb{P}(W_t = W_{t-}) = 1 \quad \text{for all } t > 0.$$

We more generally refer to [52] for an overview of the analytical properties of Lévy  $\alpha$ -stable motions and related processes, including a description of their infinitesimal generators.

A Lévy  $\alpha$ -stable motion with initial distribution  $\mu$  can be discretized as follows. For  $\Delta \in (0, 1)$ , define the Markov chain  $(u_k^\Delta)_{k \geq 0}$  by  $u_0^\Delta \sim \mu$ , and  $u_{k+1}^\Delta - u_k^\Delta \sim \mathcal{S}_\alpha(\Delta^{1/\alpha})$  independently for all  $k \geq 0$ . Then by writing  $(W_t^\Delta)_{t \geq 0}$  for the appropriately-scaled, piecewise constant càdlàg process stemming from the Markov chain  $(u_k^\Delta)_{k \geq 0}$ , i.e.

$$W_t^\Delta := u_{\lfloor t/\Delta \rfloor}^\Delta,$$

it is easy to verify using the basic properties of stable distributions along with (2.3) that  $\lim_{\Delta \rightarrow 0^+} W^\Delta = W$  in the sense of finite-dimensional distributions, i.e.

$$\lim_{\Delta \rightarrow 0^+} \mathbb{E}[h(W_{t_1}^\Delta, \dots, W_{t_n}^\Delta)] = \mathbb{E}[h(W_{t_1}, \dots, W_{t_n})],$$

for all finite  $\{t_1, \dots, t_n\} \subset [0, \infty)$  and bounded and continuous functions  $h: \mathbb{R}^n \rightarrow \mathbb{R}$ .

An alternative way to construct such a discretization, localized to a finite interval, is to partition the interval by  $N$  equispaced points, and define the unnormalized density function of  $\mathbf{u} := (u_i)_{i=1}^N$  on these points as

$$(2.4) \quad \pi(\mathbf{u}) \propto \mu(u_1) \prod_{i=2}^N f(u_i - u_{i-1}; \alpha, \sigma),$$

where  $\mu$  is the initial distribution of the process  $(W_t)_{t \geq 0}$  above and  $f(\cdot; \alpha, \sigma)$  stands for the stable density function with stability index  $\alpha$  and appropriately-chosen scale parameter  $\sigma$ .

It has recently been shown in [14] that a certain class of  $\alpha$ -stable priors (including the Lévy  $\alpha$ -stable motion) for Bayesian inverse problems are discretization invariant, in the sense that the posteriors corresponding to the finite-dimensional discretized priors converge to the infinite-dimensional posterior corresponding to the original  $\alpha$ -stable process. This is an attractive property for numerical edge-preserving inversion, and in stark contrast to finite-variance priors, whose discretizations always converges to a Gaussian process.

The only two-dimensional  $\alpha$ -stable field we consider in this paper is a simple generalization of the quasi-isotropic Cauchy first order difference prior [54], defined analogously to (2.4). That is, the probability density function of an  $\alpha$ -stable random field  $\mathbf{u}$  discretized through finite differences on a two-dimensional rectangular domain  $\Omega \subset \mathbb{R}^2$  is proportional to

$$(2.5) \quad \pi(\mathbf{u}) \propto \pi_{\partial\Omega}(\mathbf{u}_{\partial\Omega}) \prod_{i,j \notin \partial\Omega} f_B(u_{i,j} - u_{i,j-1}, u_{i,i} - u_{i-1,j}; \alpha; \sigma),$$

where  $\partial\Omega$  denotes the set of the left and bottom indices on the grid, and  $f_B(\cdot, \cdot; \alpha, \sigma)$  the symmetric bivariate  $\alpha$ -stable probability density function. The probability density function  $\pi_{\partial\Omega}$  is applied on the grid points at the left and bottom boundary of the grid to make the resulting distribution of  $\mathbf{u}$  proper.

**2.3. Hierarchical  $\alpha$ -stable priors.** Hierarchical priors are dominantly used within Gaussian priors [19, 59, 5]. With these priors, we can model discontinuities and other features with varying scale or smoothness at the target function. Unfortunately, the computational complexity of the canonical Gaussian priors is cubic with respect to the number of training points, unless a special formulation of the process is employed, like a stochastic partial differential equation [35]. The hierarchical priors might require several layers on top of each other to perform well, while having too many layers may not offer any additional expression capability [22] but rather overfit to the data.

We aim to construct and demonstrate simple two-layer Markovian hierarchical  $\alpha$ -stable priors that might prove useful without the same computational or implementation complexity of the hierarchical Gaussian processes. We model the scale or the stability of a discretized  $\alpha$ -stable process as another  $\alpha$ -stable process. This is possible due to the simple Markovian construction of the first order difference prior, that effectively allows expressing the normalization constant of the joint distribution of the discretized process and its parameters processes in a closed form. Specifically, a hierarchical  $\alpha$ -stable difference process  $\mathbf{u}$  with scale  $\sigma = G(c)$  and stability  $\alpha = H(s)$  being both based on other discretized  $\alpha$ -stable difference processes,

could be constructed as follows:

$$(2.6) \quad \begin{aligned} \pi(\mathbf{u}, \mathbf{c}, \mathbf{s}|\mathbf{y}) &\propto \pi(\mathbf{y}|\mathbf{u})\pi(\mathbf{u}|\mathbf{c}, \mathbf{s})\pi(\mathbf{c})\pi(\mathbf{s}) = \\ &\pi(\mathbf{y}|\mathbf{u})f\left(u_1; H(s_1), G(c_1)\right)f(c_1; \alpha_c, \sigma_c)f(s_1; \alpha_s, \sigma_s) \\ &\cdot \prod_{i=2}^N f\left(u_i - u_{i-1}; H(s_i), G(c_i)\right)f(c_i - c_{i-1}; \alpha_c, \sigma_c)f(s_i - s_{i-1}; \alpha_s, \sigma_s), \end{aligned}$$

where  $H$  and  $G$  are nonlinear functions with  $\text{Range}(G) \subseteq \mathbb{R}^+$ , and  $\text{Range}(H) \subseteq (0, 2]$ .  $f(\cdot; \alpha, \sigma)$  denotes the probability density function of a univariate  $\alpha$ -stable random variable with stability  $\alpha$ , scale  $\sigma$ , and skewness parameter  $\beta = 0$ . The conditional distribution  $\pi(\mathbf{u}|\mathbf{c}, \mathbf{s})$  integrates to a constant, regardless of  $\mathbf{c}$  and  $\mathbf{s}$ , as do the priors  $\pi(\mathbf{c})$  and  $\pi(\mathbf{s})$ , since  $\sigma_s, \sigma_c, \alpha_s$  and  $\alpha_c$  are fixed. The overall joint prior distribution is thus proper.

To the best of our knowledge, the convergence properties of the hierarchical  $\alpha$ -stable processes in the continuous-time limit are unknown – a sum of two Lévy  $\alpha$ -stable random variables with different stability indices does not obey an  $\alpha$ -stable distribution. However, continuous-time processes with local stability index varying with the state of the process, commonly called *stable-like processes*, are well-studied in the literature; see e.g. Chapter 7 in [30] and Theorem 5.2 in [31].

Further studies are thus needed regarding the matter, but as we demonstrate in the numerical experiments, the hierarchical  $\alpha$ -stable process constructions are promising. Unfortunately, the presented hierarchical priors cannot be applied to the  $\alpha$ -stable difference priors when the spatial dimension greater than one. That is because the normalization constant of the priors are intractable due to their construction upon the distributions of increments between nearest neighbors. However, a Matérn-like stochastic partial differential equation prior could be optionally employed instead of the difference priors [54], what would effectively allow incorporating deep  $\alpha$ -stable processes thanks to the tractable normalization constants.

### 3. APPROXIMATION OF $\alpha$ -STABLE PROBABILITY DENSITY FUNCTIONS

We provide a brief literature overview on existing methods approximating  $\alpha$ -stable density functions. Afterwards we present our hybrid method for the approximation, which we subsequently deploy in the numerical experiments section. Various relative error bounds for the probability density approximations are provided. For simplicity, we denote with  $r$  both the argument of the univariate probability density functions, and the Euclidean distance of the arguments of the multivariate  $\alpha$ -stable probability density functions to the origin.

Unless otherwise indicated, the approximations are applied for  $\sigma = 1$ . Recall that for general symmetric  $\alpha$ -stable laws, the probability density functions for the other scale parameters are given by  $f(r; \alpha, \sigma) = \frac{1}{\sigma^d} f\left(\frac{r}{\sigma}; \alpha, 1\right)$ , where  $d$  stands for the dimensionality of the distribution [45].

A canonical method to approximate the  $\alpha$ -stable probability density functions is to evaluate the inverse Fourier transform of the characteristic function. For the symmetric univariate  $\alpha$ -stable distributions given by (2.1) with  $\sigma = 1$ , the probability density function can be expressed as [44]

$$(3.1) \quad f(r; \alpha) = \frac{1}{\pi} \int_0^\infty \cos(rt) \exp(-t^\alpha) dt.$$

In theory, numerical integration allows evaluating the density of any  $\alpha$ -stable distribution at an arbitrary point  $r$  with specified precision. The integral may be impractical to evaluate for large  $r$  and small  $\alpha$  due to the severe oscillations [44], so oscillatory integral techniques have been proposed to address the issue [3].

Additionally, there is an alternative integral representation formula [46], that we call Nolan's method for short, for the univariate  $\alpha$ -stable density function when  $\alpha \neq 1$ . For simplicity, if we consider the case  $\beta = 0$  and  $\alpha \neq 1$ , the law for an  $\alpha$ -stable random variable with  $\mu = 0$  and  $\sigma = 1$  given by the method is [46]

$$(3.2) \quad f(r; \alpha) = \frac{\alpha |r|^{\frac{1}{\alpha-1}}}{\pi |\alpha - 1|} \int_0^{\pi/2} Q(t, \alpha) \exp(-|r|^{\frac{\alpha}{\alpha-1}} Q(t, \alpha)) dt,$$

where  $Q(t, \alpha) = \left( \frac{\cos(t)}{\sin(\alpha t)} \right)^{\frac{\alpha}{\alpha-1}} \frac{\cos(\alpha t - t)}{\cos(t)}$ . In contrast to the inverse Fourier method, the integrand in Nolan's method is compactly supported and non-oscillatory. Unfortunately, the integrand becomes extremely peaky and narrow when  $|\alpha - 1| < 0.02$ , and then the method is unpractical to use unless arbitrary precision arithmetic is used for the integration [46]. Thus, the univariate symmetric  $\alpha$ -stable laws can be accurately evaluated with either Nolan's method or the inverse Fourier transform method depending on the values of  $\alpha$  and  $r$ . The approximation methods based on the Fast Fourier transform [53, 6, 38] are also worth mentioning. They are simple to implement and relatively fast to evaluate, but must be used in conjunction with interpolation to approximate the density at a point which is not part of the FFT grid. It has been reported that the FFT based approximation is accurate only for large  $\alpha$  [10].

The approximations based on the integral representations of  $\alpha$ -stable laws are complemented by series expansions. A well-known series expansion for the univariate  $\alpha$ -stable density is of form [8]

$$(3.3) \quad f(r; \alpha) \sim -\frac{1}{\pi} \sum_{k=1}^{\infty} \frac{(-1)^k \Gamma(k\alpha + 1) \sin\left(\frac{k\pi\alpha}{2}\right)}{k!} r^{-k\alpha-1},$$

which is an asymptotic expansion for  $\alpha \in (1, 2)$  for  $r \rightarrow \infty$ , and converges pointwise to the true density for  $\alpha \in (0, 1)$ . There is a similar series expansion, also outlined in [8], which is an asymptotic series for  $\alpha \in (0, 1)$  and a converging series for  $\alpha \in (1, 2)$  at  $r \rightarrow 0^+$ . Furthermore, there exist methods that provide a converging series approximation for the symmetric univariate probability densities for  $\alpha \in (0, 2)$  by combining two separate series expansions [11], or approximate the inverse Fourier transform of the characteristic function by domain splitting and implementing different series expansions within them [18].

The methodology for approximating spherically contoured multivariate  $\alpha$ -stable distributions is similar to the univariate one. There are several integral expressions for their probability density functions (see e.g. [45]), such as

$$(3.4) \quad f_M(r; \alpha_M) = \frac{2^{1-d/2}}{\Gamma(d/2)} \int_0^{\infty} (rs)^{\frac{d}{2}} J_{d/2-1}(rs) \exp(-s^\alpha) ds,$$

where  $J_\nu$  is the Bessel function of the first kind and  $r := |\mathbf{r}|$ . Analogously to the univariate case, multivariate spherically contoured  $\alpha$ -stable laws have an absolutely converging series expansion for  $r > 0$  and  $\alpha \in (0, 1)$ , which is an asymptotic expansion for  $\alpha \in (1, 2)$  and  $r \rightarrow \infty$  [45]:

$$(3.5) \quad f_M(r; \alpha) \sim \frac{-1}{2\pi^{d/2+1}} \sum_{k=1}^{\infty} \frac{(-1)^k \Gamma\left(\frac{k\alpha+2}{2}\right) \Gamma\left(\frac{k\alpha+d}{2}\right) \sin\left(\frac{k\alpha\pi}{2}\right)}{k!} \left(\frac{r}{2}\right)^{-(k\alpha+1)}.$$

Likewise, there is an absolutely converging series expansion for  $r > 0$  and  $\alpha \in (1, 2)$ , which is an asymptotic expansions for  $\alpha \in (0, 1)$  and  $r \rightarrow 0^+$  [45].



**3.1. Hybrid method for approximating  $\alpha$ -stable laws.** None of the presented approximation method is suitable to be used within Bayesian inversion. The asymptotic series expansions are fast to evaluate, but not accurate enough or even applicable for all  $r$ , not to mention  $\alpha$ . The presented numerical integration methods and the advanced series expansions [18, 11] are too time-consuming to perform within Bayesian continuous-parameter estimation, since the probability density functions must be evaluated up to several hundreds of thousands of times even in the modest-dimensional settings.

To address the issues, our hybrid approximation method is two-part. When  $r$  is small, we approximate the  $\alpha$ -stable laws with two-variable bicubic splines that are fitted on grids of precomputed  $\alpha$ -stable log-densities with varying radius  $r$  and stability  $\alpha$ . We employ the Julia library `Interpolations.jl` to evaluate the bicubic splines. The densities within the grid nodes are computed through the direct integral method (3.1) and Nolan's method (3.2). Additionally, an asymptotic series expansion of (3.3) is employed for the tails when  $r$  is large in the case of univariate  $\alpha$ -stable laws. The methodology is the same for the bivariate symmetric  $\alpha$ -stable laws, as we use the integral expression with the Bessel function in (3.4) to build the spline grids, and (3.5) for the tail approximations. We use three terms in the series expansion approximations. The first bicubic spline grid of precomputed log-densities is applied when  $r \in [0, 0.9]$ ,  $\alpha \in [0.5, 1.9]$ . We divide the domain  $[0, 1.0] \times [0.5, 1.9]$  uniformly to the intervals of  $h_r = 0.01$  and  $h_\alpha = 5 \cdot 10^{-4}$ , and evaluate numerically the densities using the integral methods. When  $|\alpha - 1| < 0.2$ , the Fourier integral is used from (3.1), otherwise we employ the Nolan's method of (3.2). Even though it is reported the Nolan's method works for  $|\alpha - 1| \geq 0.02$ , the integrand in can be still difficult to evaluate numerically, since the domain of integration should be evaluated in parts near the peak of the integrand. The peak is located at  $t_p$  which satisfies the equation  $Q(t_p, \alpha)|r|^{\frac{\alpha}{\alpha-1}} = 1$  [46]. Instead of introducing improvised heuristics for the integration and domain splitting, we count on the Fourier integral for the aforementioned stability values that are tricky in Nolan's method. The numerically evaluated densities of both of the methods agree which each with a least 12 decimals for  $|\alpha - 1| \geq 0.2$ , so even using only the Fourier approach would be enough for our needs.

The second bicubic spline grid is constructed in  $r \in [0, 30]$ ,  $\alpha \in [0.5, 1.9]$ . We use the same grid node spacings of  $h_r = 0.01$  and  $h_\alpha = 5 \cdot 10^{-4}$  in the domain  $[0, 30] \times [0.5, 1.9]$  for precomputation of the log-densities, and use Nolan's method for approximating the densities when  $|\alpha - 1| > 0.2$ . However, we limit the usage of the spline only for  $r \in (0.9, 29.6)$ ,  $\alpha \in [0.5, 1.9]$ . In fact, the third bicubic approximation is employed for  $r \in [29.6, 30]$ ,  $\alpha \in [0.5, 1.9]$ . We call this region as the transition region of the approximation. Let us denote  $r_a := 29.6$ ,  $r_b = 30.0$ , and  $\Delta = r_b - r_a$ . Let the log-density approximation given by the asymptotic series expansion from Equation (3.3) at the spline grid node  $r_a, \alpha_j$  be  $f_{a,j}^s$  and its derivative with respect to  $r$  be  $D_{a,j}^s$ . Additionally, let the approximation given by the numerical integration at  $r_b, \alpha_j$  be  $f_{b,j}^d$ , and its derivative with respect to  $r$  by  $D_{b,j}^d$ . We set the value in the transition region spline grid point value at  $i, j$  to follow an auxiliary cubic Hermite interpolation as follows:

$$(3.6) \quad f_{i,j} = \frac{(3\Delta q_i^2 - 2q_i^3)}{\Delta^3} f_{b,j}^s + \frac{(\Delta^3 - 3\Delta q_i^2 + 2q_i^3)}{\Delta^3} f_{a,j}^d + \frac{q_i^2(q_i - \Delta)}{\Delta^2} D_{b,j}^d + \frac{q_i(q_i - \Delta)^2}{\Delta^2} D_{a,j}^s,$$

where  $q_i := r_i - r_a$ . Equation (3.6) is applied for each stability  $\alpha_j$  within the transition grid separately. The Hermite interpolation is only applied during the



construction of the transition interpolation spline, because the evaluation of the constructed grid is performed by the bicubic spline library in Julia. Introducing the Hermite interpolated data points as an additional step at the transition region helps to avoid abrupt changes in the derivatives of the log-densities near the boundary of the transition region and the tail approximation, although we enforce  $C^1$  continuity of the overall log-density approximation. The  $C^1$  continuity is enforced by setting the values of derivatives with respect to  $r$  on the boundary  $r = 0.9$  on the first spline to agree with the second spline. The derivatives with respect to  $r$  on the boundaries  $r = 29.6$  and  $r = 30.0$  of the third spline are set to follow the values given by the second spline and the tail approximation, respectively. On the second spline, the second order derivatives with respect to  $r$  are set to zero. The splines for  $r \in [0, 0.9]$  and  $r \in [29.6, 30.0]$  are used because the resulting systems of equations of the spline coefficients involving non-zero boundary conditions are smaller, and hence easier to solve than directly incorporating them into the coefficients of the largest spline grid.

The overall approximation method is depicted in Figure 1. We do not consider the cases  $\alpha < 0.5$  or  $\alpha > 1.9$ . Low stability values are not in our interest, and including them would require increasing the number of nodes in the precomputed log-probability density grids to sustain the accuracy of the approximation. Likewise, our error estimates for the approximation would grow significantly, and the asymptotic series expansions would need to be evaluated way further from the origin than the current threshold of  $r > 30$ , if  $\alpha$  was very close to 2. The same interpolation methods and region partitioning are employed for both the univariate and bivariate symmetric  $\alpha$ -stable log-probability densities. Evaluation of an  $\alpha$ -stable log-density takes approximately 100 nanoseconds in the domain of the spline grids, and about 400 nanoseconds in the asymptotic tail expansions on a workstation equipped with Intel Xeon CPU E5-2698 v4 central processing unit.

**3.2. Error bounds of the approximation.** To derive the error bounds for our hybrid approximation method, we assume the integration error of the probability densities as zero within the spline grid points. For simplicity, we ignore the transition region from the error estimates as it can be anyway left out from the method with the expense of having less regular approximation, respectively. Then we make use of the properties of bicubic splines as follows. The error estimates below can be found in [26].

**Theorem 3.1.** *Write  $f_T := f(r; \alpha)$  for the (true) density of the symmetric  $\alpha$ -stable distribution with  $\sigma = 1$ , and by  $f_A := f_A(r; \alpha)$  the bicubic spline interpolation described above. The error caused by the bicubic spline approximation can then be approximated by [12, 26]*

$$(3.7) \quad \begin{aligned} \|\log f_T - \log f_A\|_\infty &\leq \frac{5}{384} \|(\log f_T)^{(4,0)}\|_\infty h_r^4 + \frac{81}{64} \|(\log f_T)^{(2,2)}\|_\infty h_r^2 h_\alpha^2 \\ &\quad + \frac{5}{384} \|(\log f_T)^{(0,4)}\|_\infty h_\alpha^4, \end{aligned}$$

where  $h_r$  and  $h_\alpha$  stand for the lengths of the log-density interpolation grid cells in the directions of the radius and the stability index respectively, and the superscripts  $(i,j)$  stand for partial derivatives of the form  $\frac{\partial^{i+j}}{\partial r^i \partial \alpha^j}$ .

Estimating the partial derivatives of  $\log f_T$  appearing in the suprema in (3.7) involves estimating the partial derivatives of  $f_T$  from above, and  $f_T$  itself from below. Both types of estimate are tricky to do in a precise manner, due to the lack of any sort of a closed-form expression for  $f_T$ . We will make use of several strategies which are variably efficient for different regions of  $(r; \alpha)$  when estimating the partial derivatives of  $f_T$ , and subsequently use the first-order variants of these

estimates in conjunction with a precomputed grid (similar to the one detailed in the context of spline approximations above) and the fundamental theorem of calculus for the lower bounds of  $f_T$ . The full details of these estimates are presented in the Supplementary Material, but we give a taste of the methodology and results here, starting with the univariate case.

First, we can obtain crude uniform bounds (with respect to  $r$ ) for each  $(f_T)^{(i,j)}$  by e.g. differentiating (3.1) under the integral sign and eliminating the resulting oscillatory term simply using the triangle inequality. We can somewhat refine this pointwise for “moderate”  $r > 1$  by using standard oscillatory integral techniques (which basically amount to partial integration against a sufficiently quickly vanishing function, resulting in an upper bound of order  $r^{-1}$ ). This is largely the best we can do for moderate values of  $r$ , where neither of the asymptotic expansions (see (3.3) and the subsequent discussion) come close to approximating  $f_T$  well with only a couple summands – the region of said “moderate” values will of course depend on  $\alpha$ .

For larger values of  $r$ , we may exploit the expansion (3.3) pointwise with e.g. 2–3 summands and an explicit (albeit complicated) expression for the remainder term, due to Bergström [8]. Some of the integrals we encounter here (corresponding to the remainder term, particularly with partial derivatives with respect to  $\alpha$ ) are highly intractable in the mathematical sense of the word, but non-oscillating and well-behaved enough for efficient numerical estimation, yielding an upper bound that decreases to an order roughly comparable to that of  $f_T$  for  $r \rightarrow \infty$ , and where the asymptotic constants stay sufficiently tame for  $\alpha \in [0.5, 1.9]$ . This all holds, *mutatis mutandis*, for  $r \rightarrow 0^+$  as well.

We thus obtain several different kinds of upper bounds for  $|(f_T)^{(i,j)}(r; \alpha)|$ , pointwise with respect to  $(r, \alpha)$ . With some minor additional work, we may loosen the estimates very slightly so that they will be uniform for  $r \in [r_j, r_{j+1}]$  and  $\alpha \in [\alpha_i, \alpha_{i+1}]$ , where

$$\bigcup_{i,j} [\alpha_i, \alpha_{i+1}] \times [r_j, r_{j+1}] = [0.5, 1.9] \times [0, 30],$$

is a tiling of the relevant parameter space with  $r_{j+1} - r_j = \alpha_{i+1} - \alpha_i = \Delta > 0$ . Here  $\Delta$  stands for a (sufficiently small) discretization parameter;  $\Delta = \frac{2}{10^3}$  in our numerical simulations.

With the above upper estimates for the partial derivatives of  $f_T$ , we are in a place to estimate  $f_T$  from below with reasonable accuracy. Namely, noting that  $f_T(r; \alpha)$  is for fixed  $\alpha$  always a decreasing function of  $r$ , we may precompute  $f_T(r_j; \alpha_i)$  at the nodes of the discretized grid, and thus use the fundamental theorem of calculus to obtain

$$\begin{aligned} \inf_{\alpha_i \leq \alpha \leq \alpha_{i+1}, r_j \leq r \leq r_{j+1}} f_T(r; \alpha) &\geq \min(f_T(r_{j+1}; \alpha_i), f_T(r_{j+1}; \alpha_{i+1})) \\ &\quad - \frac{\Delta}{2} \sup_{\alpha_i \leq \alpha \leq \alpha_{i+1}, r_j \leq r \leq r_{j+1}} (f_T)^{(0,1)}(r; \alpha). \end{aligned}$$

The discussion above also applies to the bivariate case, with the additional difficulty of the Bessel function of the first kind  $J_0$  in the representation (3.4). In the Supplementary Material, we present analogous asymptotic expansions with respect to  $r \rightarrow 0^+$  and  $r \rightarrow \infty$  with quantitative remainder term estimates. In particular for  $r \rightarrow \infty$ , we present a modification of Bergström’s [8] complex-analytical treatment, which allows us to obtain estimates for the remainder term in the bivariate case which are not immediate from the asymptotic expansions presented in [45].

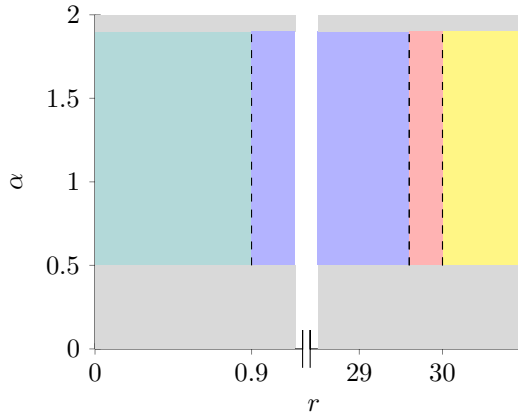


FIGURE 1. Regions of the hybrid interpolation method for approximating symmetric  $\alpha$ -stable laws. Turquoise: the first bicubic interpolation grid. Violet: the second bicubic interpolation grid. Red: the transition region of the spline and the asymptotic series. Yellow: the asymptotic series expansion for  $r \rightarrow \infty$ . Gray: the implemented approximation method is not employed.

For the univariate  $\alpha$ -stable log densities, the obtained bounds for the partial derivatives lead to the final absolute error estimates of

$$\sup_{r \leq 30, 0.5 \leq \alpha \leq 1.9} |\log f_T(r; \alpha) - \log f_A(r; \alpha)| \leq \begin{cases} 0.00038 & (\text{univariate case}); \\ 0.22 & (\text{bivariate case}). \end{cases}$$

The accuracy of the approximations are enough for our needs. The error estimate for the bivariate log-density is orders of magnitudes higher than for the univariate one due to the significantly larger suprema for the partial derivatives within the domain of the splines, particularly with small  $\alpha$ . If the lower bound of  $\alpha$  of the approximation domain was increased to 0.7, the bivariate log-density error estimate would be decreased to 0.013, accordingly.

For the relative error bounds of tails, we have the following estimates. Denoting by  $\mathcal{S}_3(r; \alpha)$  the sum in (3.3) (resp. (3.5)) with 3 in place of  $\infty$ , and by  $f_T(r; \alpha)$  the true density, we have

$$\sup_{r > 30, 0.5 \leq \alpha \leq 1.9} |\log f_T(r; \alpha) - \log \mathcal{S}_3(r; \alpha)| \leq \begin{cases} 0.00097 & (\text{univariate case}); \\ 0.0017 & (\text{bivariate case}). \end{cases}$$

These estimates are also detailed further in the appendix.

#### 4. NUMERICAL EXAMPLES

We demonstrate the  $\alpha$ -stable priors in three numerical experiments. We employ the priors first in a deconvolution, which is a well-known linear inverse problem. Moreover, the same priors are used in estimating the conductivity field of an elliptic PDE in two spatial dimensions. For now, we use only MAP-estimators in the reconstructions, because full Bayesian inference with the presented random field priors requires usage of MCMC methods that has been shown to struggle with such heavy-tailed priors [54]. Since the assessment of the reconstructions in inverse problems cannot be usually accomplished in a unified manner, we do not intentionally tabulate any metrics of the reconstructions, such as  $L^2$  errors of the reconstructions, in the manuscript. The Julia codes of the experiments can be found from <https://github.com/suurj/alpha-stable>.

**4.1. MAP estimation.** Evaluation of the MAP estimates (Equation (1.2)) in Bayesian continuous-parameter estimation is usually performed with the help of a nonlinear conjugate gradient algorithm, a quasi-Newton method, a matrix-free truncated Newton method or a combination of them [2, 27, 40, 58]. Thanks to their generality, the methods are applicable for both linear and nonlinear inverse problems. Additionally, the methods do not require the exact full Hessian of the objective function to be evaluated unlike the standard Newton method does, what is crucial from a computational perspective. Under certain assumptions regarding the convexity of the objective function and its Hessian-gradient products, the standard Newton method is quadratically convergent, while the quasi-Newton methods are asymptotically superlinearly convergent [49], and the nonlinear conjugate gradient method is either linearly or superlinearly convergent depending on how the algorithm is initialized [47]. Hence, a quasi-Newton method such as the limited-memory Broyden–Fletcher–Goldfarb–Shannon algorithm (L-BFGS) is often selected instead of the conjugate gradient method in large-scale convex optimization [36].

It is worth mentioning that a set of new optimization algorithms for large-scale problems have been recently proposed in the field of deep learning. Algorithms such as adaptive moment estimation (Adam) [29] have been proposed to accelerate training of neural networks [20] with large input datasets, and to alleviate the issue of over-fitting the network parameters through various ensemble training techniques. However, the optimization algorithms tailored for deep learning do not offer any noteworthy advantages over the classical optimization methods in our numerical examples, as no training or large datasets are involved.

For these reasons, maximization of the log-posteriors is done through the L-BFGS method in the deconvolution experiments. Moreover, we resort to the bounded L-BFGS algorithm [60] at inversion of the conductivity field of a linear elliptic PDE. As the numerical implementations of the limited-memory BFGS algorithms, we use `Optim.jl` [39] for the unconstrained L-BFGS, and a Julia wrapper `LBFGSB.jl` of the original Fortran-implementation of L-BFGS-B [60]. Lastly, we want to emphasize that the presented  $\alpha$ -stable random field priors often make the posteriors multimodal [54], and finding global maxima from such distributions is virtually impossible. Employing a different optimization algorithm for the MAP estimator than those used here would likely affect only the needed computational time until convergence is achieved.

**4.2. One-dimensional deconvolution.** As the first numerical experiment, we demonstrate the first order  $\alpha$ -stable difference priors with varying stability and scale. The discretized target function  $\mathbf{u}$  is divided in 500 grid points, which we evaluate with a normalized convolution kernel

$$g(s, t) = 25 \exp(-50|s - t|),$$

at 60 equispaced points within the support of the target function. Function  $\mathbf{u}$  includes both discontinuities and piecewise realizations of a Gaussian process with Matérn covariance to demonstrate the properties of the priors. Finally, we add white Gaussian noise with variance of  $0.02^2$  to the convolutions so the likelihood function of the experiment is Gaussian. In the MAP estimation, we use a matrix approximation of the convolution operator like we do in the measurement data generation step. In addition to using fixed scale and stability in the first order  $\alpha$ -stable prior, we also consider them as functions to be estimated as well through the hierarchy defined in Equation 2.6. The ground truth function is plotted in Figure 2, and the reconstructions in Figures 2, 3, 4 and 5. For all the MAP estimates, we use equispaced grids with 120 points. This implies the posterior distribution is 360-dimensional if both the scale and the stability are considered as processes.

The MAP estimates with the non-hierarchical  $\alpha$ -stable first order difference priors in Figure 2 demonstrate the effect of altering the stability  $\alpha$  or scale  $\sigma$  of the distribution of the increments in the prior. As a rule of thumb, the smaller the stability  $\alpha$  is, the stronger the prior favors non-Gaussian increments, so they are usually close to zero. The larger the scale  $\sigma$  is, the greater the variability is allowed within the increments. Stability values for  $1 \leq \sigma \leq 2$ , are particularly useful for reconstructing the target function in this case. Those priors are able to favor the existence of Gaussian-like parts of the ground truth function when needed. If the estimation was done using stationary Gaussian priors, the MAP estimate would be either over-smoothed and incapable to locate the discontinuity at the boxcar, or it could detect the discontinuity at the expense of being very sensitive to noise.

Considering the stability of the prior as another first order  $\alpha$ -stable process, turned out to be less successful. We let the scale of the process  $\mathbf{u}$  to follow an  $\alpha$ -stable process with scale  $\sigma = 0.01$ , and set its untransformed stability process  $\mathbf{s}$  to follow an  $\alpha$ -stable process with the parameters tabulated in Figure 3. To guarantee that  $0.51 \leq \alpha \leq 1.9$ , we apply a transformation

$$(4.1) \quad \alpha = 0.51 + 1.39S(s),$$

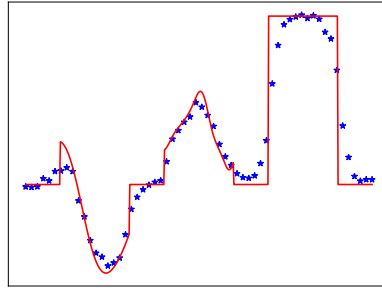
where  $S(x) = \frac{1}{1+e^{-x}}$ . In both Figures 3 and 5, the stability processes are shown in their transformed values. The stability process seems to be either close to constant ( $\approx 1.25$ ) or decreasing towards the right side of the domain in all the tabulated cases. However, there is some variation in the stability process in the middle of the domain when the untransformed process have the parameters  $\alpha = 0.8, \sigma = 0.1$ . The phenomenon may suggest that having the stability as a process does not work well as a prior. When the stability of the untransformed stability process is  $\alpha_s = 1.4$  and its scale  $\sigma_s = 0.05$  (Equation (2.6)), the reconstruction of  $\mathbf{u}$  is smooth at first, but as the stability decreases, the reconstruction becomes more discontinuous and non-Gaussian.

In the one-dimensional deconvolution experiment, the best results in terms of the reconstruction agreement with the ground truth are obtained when the scale of  $\mathbf{u}$  process is considered as a process instead of its stability. We fix the stability of  $\mathbf{u}$  to  $\alpha = 1.9$ , and instead modeled the untransformed scale process  $\mathbf{c}$  with another  $\alpha$ -stable process with parameters shown in Figure 4. The final scale process is given by

$$(4.2) \quad \sigma = 0.001 + 0.05S(c).$$

The reconstructions where the untransformed scale process have scale of  $0.05 \leq \sigma_c \leq 0.1$  and stability between  $0.8 \leq \alpha_c \leq 1.9$ , agree well with the ground truth and even with each other.

For the last, setting both the scale and the stability of  $\mathbf{u}$  as  $\alpha$ -stable processes seem to suffer from the same issue as the stability process case. Namely, either or both of the parameter processes remain close to constant throughout the domain, and the MAP estimates for  $\mathbf{u}$  are no better than in the simpler  $\alpha$ -stable priors. We set the scale of the untransformed stability index process to  $\sigma_s = 0.05$  (Equation (2.6)), and the stability of the untransformed scale parameter process to  $\alpha_c = 1.9$ . Hence, the scale parameters  $\sigma$  in Figure 5 refer to the scale of the untransformed stability process ( $\sigma_s$ ), and the the stability indices to the untransformed scale process ( $\alpha_c$ ). We transform the processes with the same sigmoid functions as in the other two cases, using Equations (4.2) and (4.1). Whether the poor reconstructions are caused by overfitting, poorly selected hyperparameters, unidentifiability, or something else, they shall be investigated.



(A) Ground truth function (red) and noisy convolutions (blue).

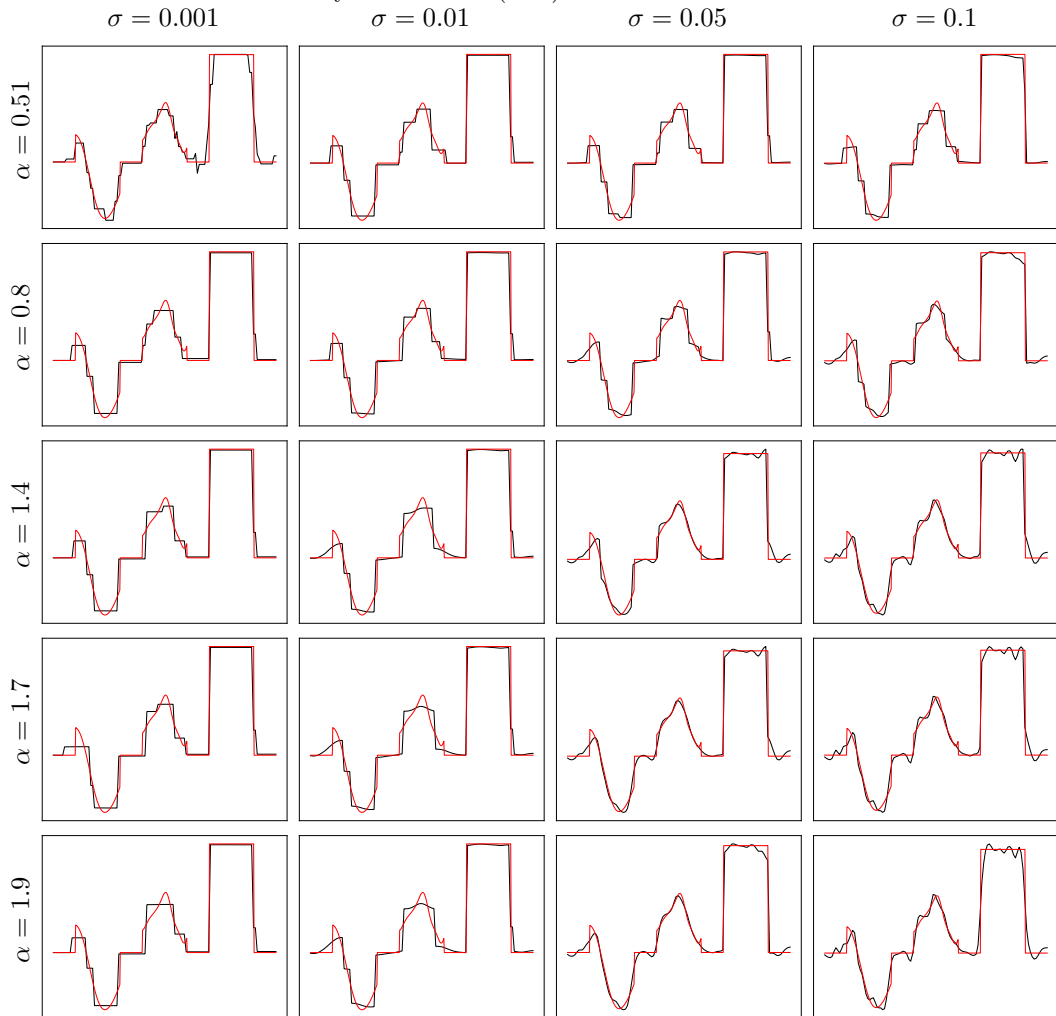


FIGURE 2. Ground truth, measurements, and the reconstructions with fixed stability and scale parameters in the one-dimensional deconvolution experiment with  $\alpha$ -stable difference prior. Red lines: ground truth. Black lines: MAP estimate for the function.

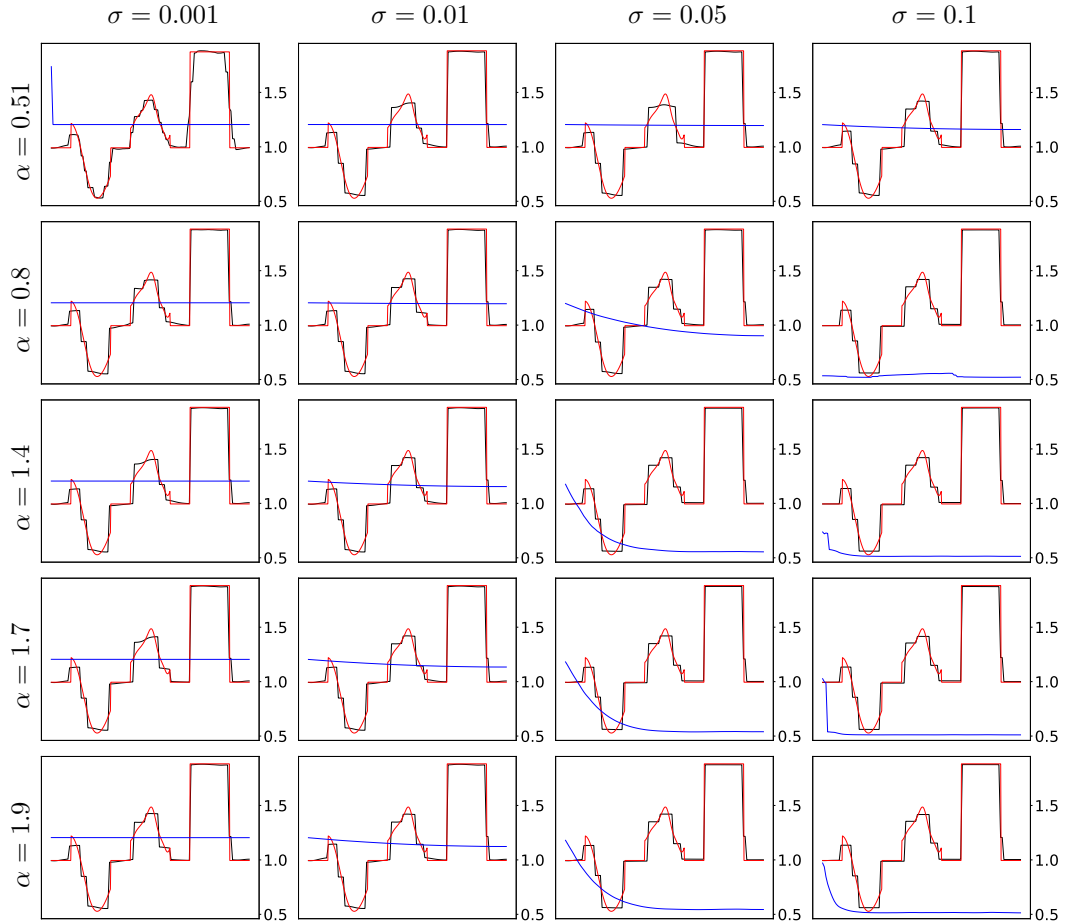


FIGURE 3. Reconstructions when considering the stability  $\alpha$  as a function. Red lines: ground truth. Black lines: MAP estimate for the function. Blue lines: MAP estimate of the stability process.

**4.3. Two-dimensional deconvolution.** We conduct a deconvolution experiment also in two dimensions. The ground truth function and the reconstructions are plotted in Figure 6. We estimate the blurred test function with the help of spherically symmetric bivariate  $\alpha$ -stable first order difference priors 2.5. The ground truth function is supported on  $[-1, 1]^2$ . It is evaluated at a uniform grid of size  $333 \times 333$ , after which the synthetic measurement dataset is approximated thorough interpolation at  $100^2$  points that are scattered according to a low-discrepancy sequence within the domain of the target function. A Gaussian convolution kernel  $h$  was employed in the blurring:

$$g(\mathbf{s}, \mathbf{t}) = \frac{150}{\pi} \exp(-150\|\mathbf{s} - \mathbf{t}\|^2).$$

The convolution is computed with a matrix approximation, like in the one-dimensional case. A grid of  $256 \times 256$  nodes is used in the MAP estimators.

The MAP estimates of the reconstructions are consistent with the one-dimensional deconvolution experiment. Increasing the stability of the  $\alpha$ -stable difference priors manifests in more Gaussian-like features in the MAP estimates. The distribution  $\alpha = 0.51$  and  $\sigma = 0.01$  is probably too spiky and heavy-tailed as the difference



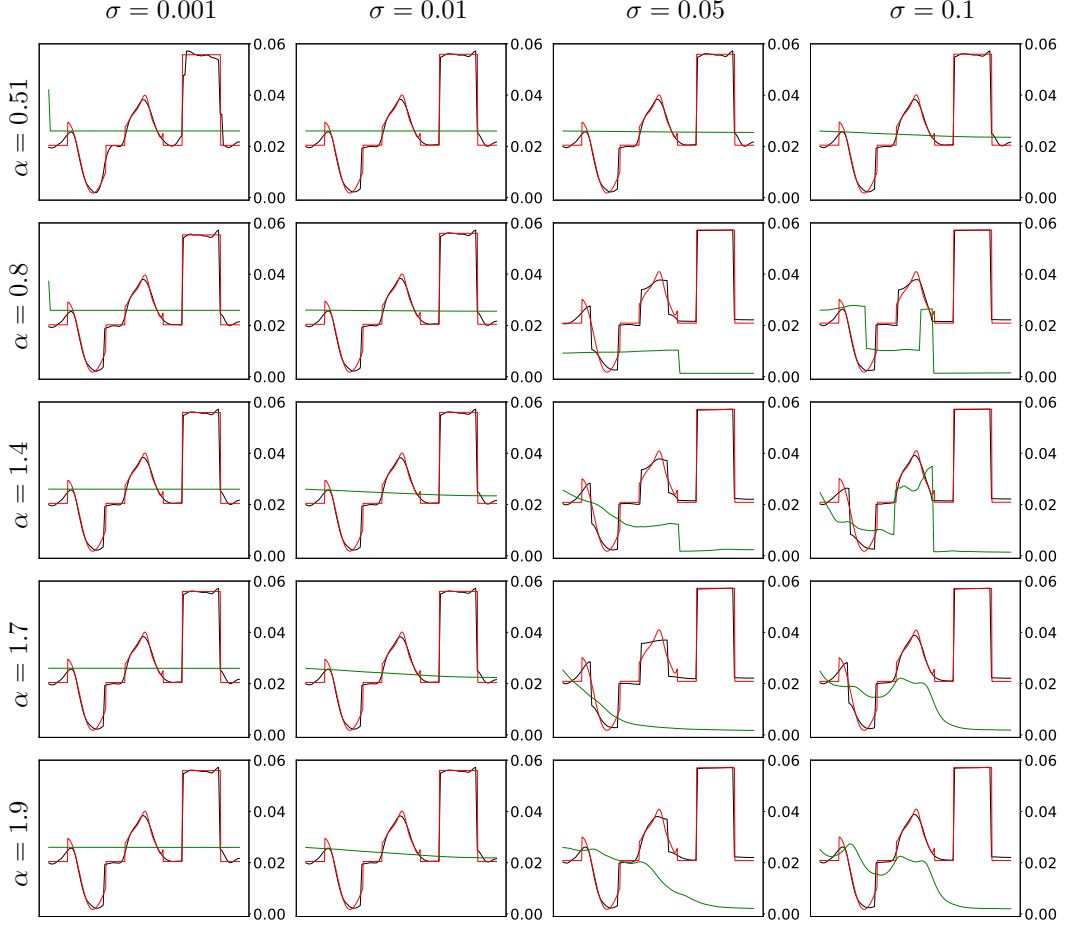


FIGURE 4. Reconstructions when considering the scale  $\sigma$  as a process. Red lines: ground truth. Black lines: MAP estimate for the function. Green lines: MAP estimate of the scale process.

prior, since the reconstruction lacks any features resembling the ground truth objects. A notable feature is the existence of diagonal discontinuities at certain MAP estimates, like in the case  $\alpha = 0.8$  and  $\sigma = 0.1$  in the object that consists of two overlapping spheres. Although the construction of the  $\alpha$ -stable difference prior incorporates bivariate symmetrically contoured  $\alpha$ -stable distributions, the prior is likely not fully isotropic. In fact, even the isotropic and upwind total variation priors are not perfectly isotropic, and a method has been proposed to alleviate the issue [17]. Unfortunately, the technique cannot be applied to the presented  $\alpha$ -stable priors, so the matter of improving the isotropicity must be considered separately.

**4.4. Inversion of an elliptic partial differential equation.** As the third numerical experiment with the  $\alpha$ -stable priors, we consider the nonlinear inverse problem of estimating a conductivity field  $k \in L^\infty(\Omega)$ , with Lipschitz domain  $\Omega \subset \mathbb{R}^2$  of an elliptic partial differential equation:

$$(4.3) \quad \begin{aligned} -\nabla \cdot (k \nabla u) &= g, & x \in \Omega \\ u &= 0, & x \in \partial\Omega, \end{aligned}$$

with prescribed zero Dirichlet boundary conditions, where  $u \in H_0^1(\Omega)$  denotes the solution of the PDE, and  $g \in L^\infty(\Omega)$ . The inversion is done using noisy observations

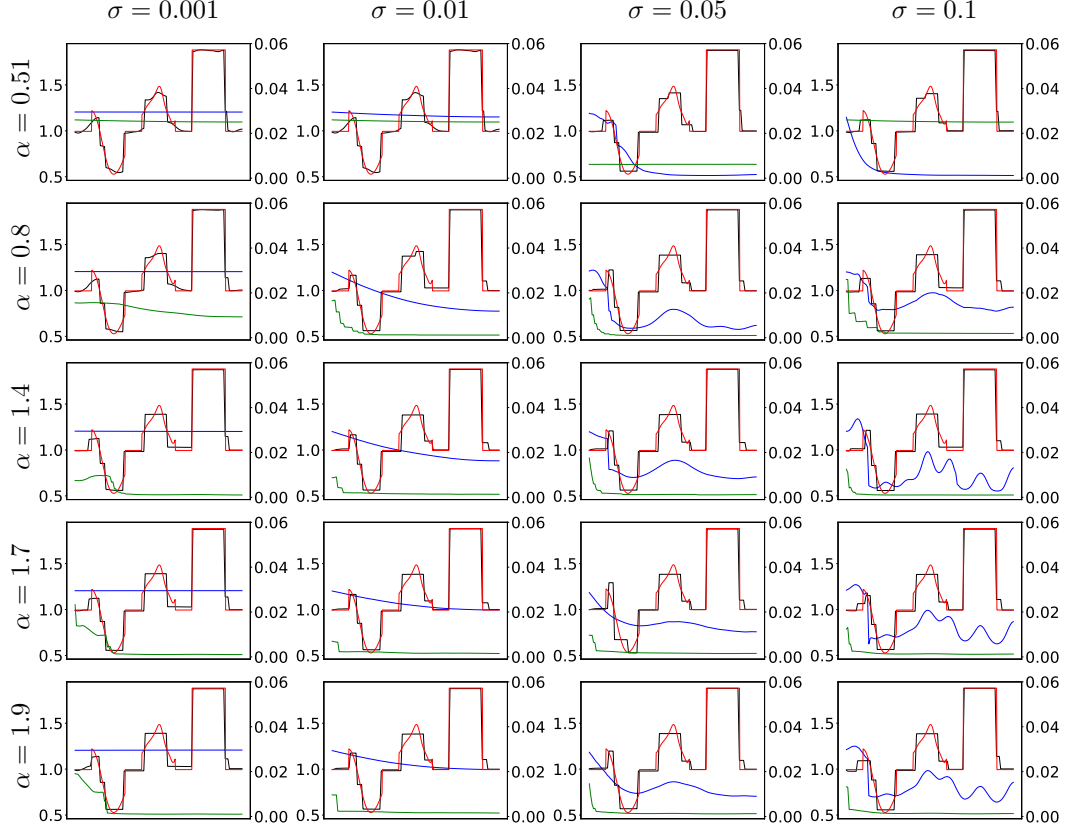


FIGURE 5. Reconstructions when considering both the stability  $\alpha$  and the scale  $\sigma$  as processes. Red lines: ground truth. Black lines: MAP estimate for the function. Blue lines: MAP estimate of the stability process. Green lines: MAP estimate of the scale process. The left axes of the subfigures stand for the stability, the right ones denote to the scale.

$\mathbf{y}$  of the solution of the PDE as the likelihood for  $k$ . We discretize the PDE with the standard centred finite difference method. The noise is assumed to be Gaussian with observations taking the form

$$(4.4) \quad y_i = u_i + \epsilon_i, \quad \epsilon_i \sim \mathcal{N}(0, 0.001^2).$$

Like in the other two experiments, we evaluate only the MAP estimator of the problem. We use a bounded limited-memory BFGS algorithm (L-BFGS-B) to calculate the MAP estimate. We employ the constraint  $10^{-5} < k < 10^2$  to ensure the well-posedness of the elliptic PDE and to keep the condition number of the matrix of the discretized system of equations for the PDE small. The gradient of the log-posterior with respect to the discretized  $k$  is calculated through a discrete adjoint method [21, 25]. That is, we solve the adjoint equation to get the adjoint  $\mathbf{q}$  through the equation

$$(4.5) \quad \left( \frac{\partial \mathbf{E}}{\partial \mathbf{u}} \right)^T \mathbf{q} = \left( \frac{\partial \pi(\mathbf{y} | \mathbf{u}(\mathbf{k}))}{\partial \mathbf{u}} \right)^T,$$

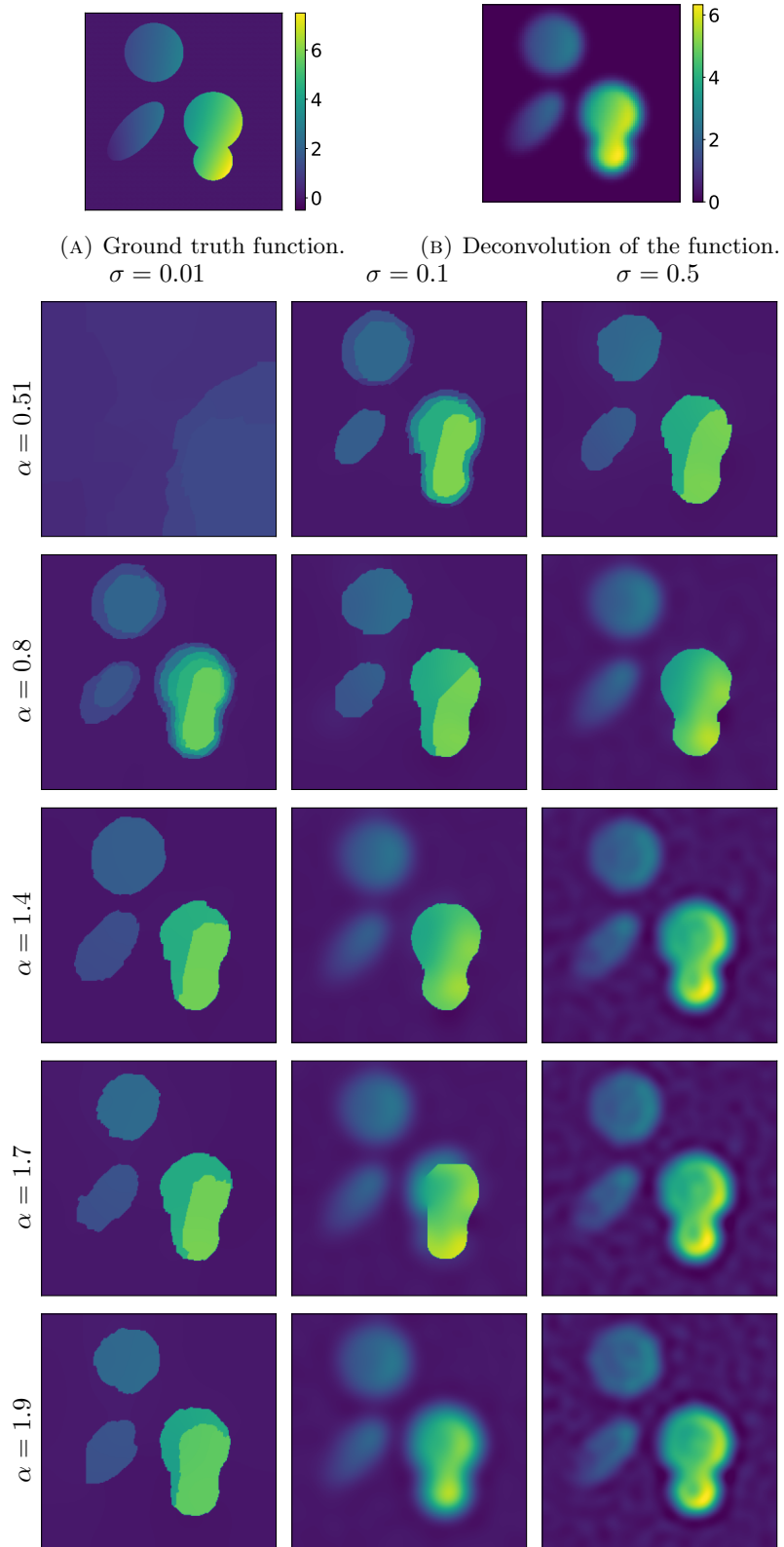


FIGURE 6. Ground truth function, its deconvolution, and the MAP estimate reconstructions of the two-dimensional deconvolution problem with  $\alpha$ -stable difference priors with varying scale  $\sigma$  and stability  $\alpha$ .

where  $\mathbf{E}$  denotes the system of finite difference equations of the discretized PDE, and  $\pi(\mathbf{y}|\mathbf{u}(\mathbf{k}))$  the Gaussian likelihood function, which merely consists of solving the PDE with given  $\mathbf{k}$  and evaluating the fidelity of the obtained solution with respect to  $\mathbf{y}$ . The gradient of the log-posterior  $\pi(\mathbf{k}|\mathbf{y})$  with respect to the discretized conductivity field  $\mathbf{k}$  is then

$$(4.6) \quad \frac{\partial \pi(\mathbf{k}|\mathbf{y})}{\partial \mathbf{k}} = -\mathbf{q} \frac{\partial \mathbf{E}}{\partial \mathbf{k}},$$

since the likelihood depends on  $\mathbf{k}$  only through  $\mathbf{u}$ .

We estimate the conductivity field with the same bivariate  $\alpha$ -stable difference priors as we do in the two-dimensional deconvolution. We use a reconstruction grid of  $128 \times 128$ . To simulate the measurements and to avoid committing an inverse crime, we calculate the solution of the PDE using a larger finite difference grid with a size of  $223 \times 223$ , and interpolate the solution at  $25 \times 25$  points that are positioned at the reconstruction grid using a low-discrepancy sequence. The source term function  $g$  of (4.3), the solution of the PDE and the ground truth conductivity, as well as the reconstructions are plotted in Figure 7.

The shape of an double-sphere object in the conductivity field is captured the best with the smaller stability indices, while the increasing the stability seems to blur the reconstruction based on the MAP estimate. On the other hand, having too large scale  $\sigma$  may make the prior uninformative. Judging by the shape and distribution of the values within the reconstruction, the prior with  $\alpha = 0.8$  and scale  $\sigma = 0.1$  could be the best out of the tested parameter choices in this case.

## 5. CONCLUSION

This work was motivated by the desire to implement approximations of the  $\alpha$ -stable random field priors for Bayesian inverse problems. Because both the Cauchy and Gaussian fields are special cases of the  $\alpha$ -stable random fields, our objective was to extend the prior selection to general  $\alpha$ -stable priors, which could prove useful in reconstructions where both Gaussian and non-Gaussian features are present. As the  $\alpha$ -stable density functions mostly lack the closed-form expressions, we introduced a computationally feasible hybrid method for approximating the symmetric univariate and bivariate  $\alpha$ -stable probability density functions. The novelty of the presented method in comparison with the existing approximation methods is its accuracy and, especially, its performance. The method allows evaluation of the  $\alpha$ -stable probability log-density functions within a stability index range of  $\alpha \in [0.5, 1.9]$  and radius argument range of  $r \in [0, \infty)$ . Furthermore, we provided error bounds for the log-density approximations.

In the numerical experiments, we employed finite-difference approximations of the  $\alpha$ -stable first order random motion priors at one- and two-dimensional deconvolution, and we also addressed the estimation of a function governed by an elliptic PDE with the same priors. The MAP estimation was implemented through the standard L-BFGS method and its bounded variant. Our objective was to illustrate how the parameters, such as the stability and scale of the  $\alpha$ -stable priors, can affect the estimation of the unknown functions. The results are promising in the sense that the presented priors are both computationally viable, manifest in useful MAP-estimates, and are yet novel compared to the existing random field priors like Gaussian, Cauchy, Besov, and total variation priors.

As we introduced new  $\alpha$ -stable priors and provided examples through MAP-estimates, we consider extending the estimators to full inference as well as other  $\alpha$ -stable priors. For future work, we will consider Bayesian neural networks [41] with  $\alpha$ -stable weights, which are possibly non-symmetric,  $\beta \neq 0$ . We believe the

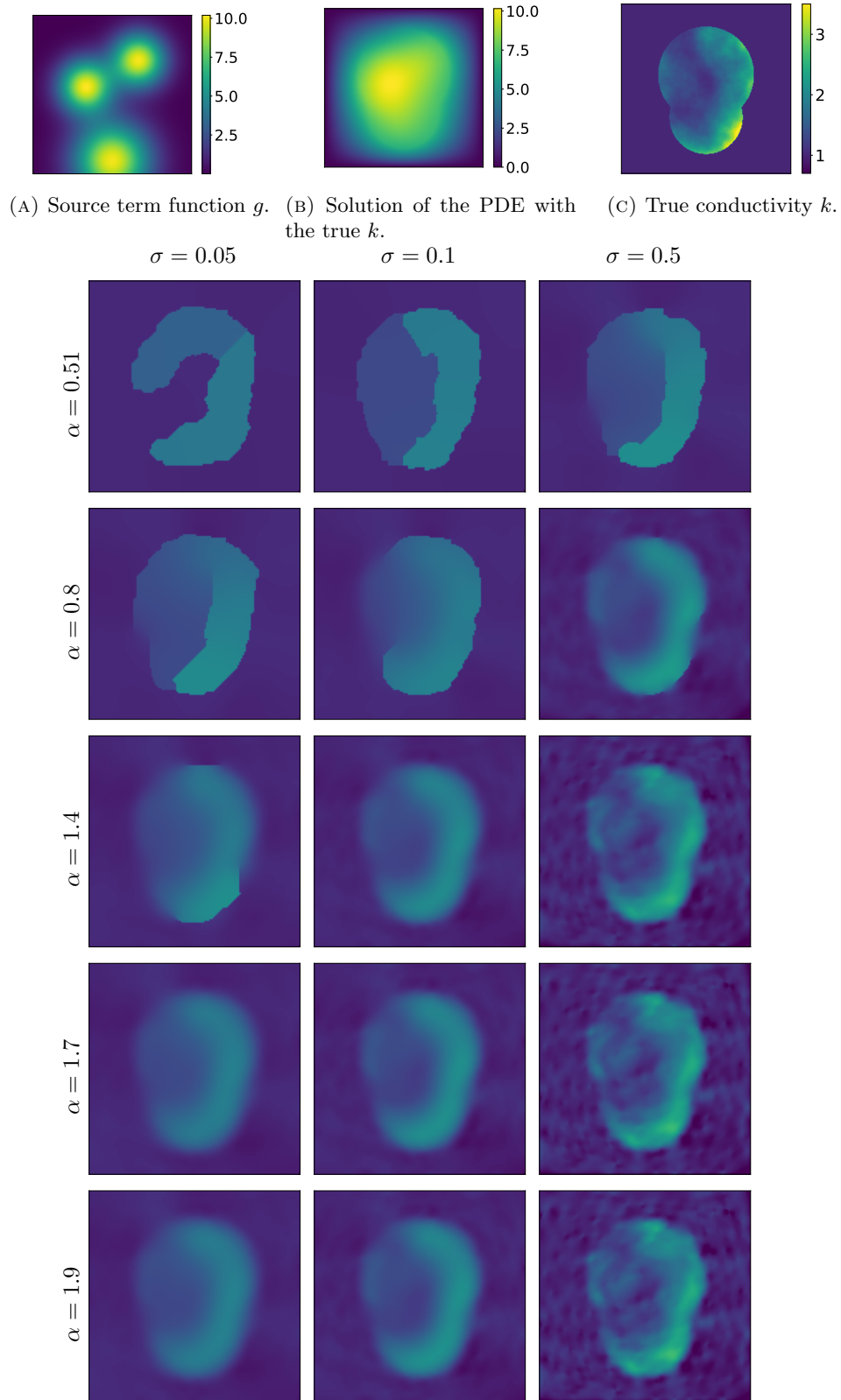


FIGURE 7. Functions employed in the nonlinear inversion of the conductivity function  $k$  of an elliptic PDE, and the MAP estimates with symmetric  $\alpha$ -stable difference priors with varying choices of the scale  $\sigma$  and stability  $\alpha$ .

developed approximations to turn out useful in that case due to the recent studies on Bayesian neural networks with Cauchy and Gaussian weights [34]. Alternatively,  $\alpha$ -stable random field approximations through the stochastic partial differential equation approach could be beneficial [9, 35, 54]. Another consideration would be to test these priors on ensemble Kalman methods [13, 15, 16], which have been used and tested with hierarchical Cauchy processes.

#### ACKNOWLEDGMENTS

We thank Sari Lasanen, Simo Särkkä and Heikki Haario for useful and interesting discussions. This work has been funded by Academy of Finland (project number 336787).

#### APPENDIX A. ERROR BOUNDS

We establish quantitative pointwise bounds for symmetric stable density functions  $f(r; \alpha)$  and their partial derivatives, based on series expansions due to Bergström.

In this appendix, the symbol  $\mathcal{R}$  stands for a generic remainder term associated to a partial series expansion of a given density function. In particular, the symbol  $\mathcal{R}$  will generally have a *different* meaning from one line to another. Its precise meaning will always be clear from context.

#### UNIVARIATE BOUNDS FOR $r \rightarrow 0$

Recall that for  $r > 0$ , the density is given by the inverse Fourier transform as follows:

$$(A.1) \quad f(r; \alpha) = \frac{1}{\pi} \int_0^\infty \cos(rt) e^{-t^\alpha} dt = \frac{1}{\pi} \Re \left\{ \int_0^\infty e^{-irt - t^\alpha} dt \right\}.$$

Let us first recall the asymptotic expansion for  $r \rightarrow 0^+$ . We may apply the Taylor series expansion for the cosine function in the first integral in (A.1), yielding

$$\begin{aligned} f(r; \alpha) &= \frac{1}{\pi} \sum_{k=0}^n \frac{(-1)^k r^{2k}}{(2k)!} \int_0^\infty t^{2k} e^{-t^\alpha} dt + \mathcal{R}(r; \alpha) \\ &= \frac{1}{\pi \alpha} \sum_{k=0}^n \frac{(-1)^k \Gamma(\frac{2k+1}{\alpha})}{(2k)!} r^{2k} + \mathcal{R}(r; \alpha), \end{aligned}$$

for any  $n \in \mathbb{N}_0$ . Since  $\|\cos^{(\ell)}\|_{L^\infty(0, \infty)} \leq 1$  for all  $\ell \in \mathbb{N}$ , we can apply Taylor's theorem and arrive at the following estimate for the remainder term:

$$|\mathcal{R}(r; \alpha)| \leq \frac{r^{2n+2}}{\pi(2n+2)!} \int_0^\infty t^{2n+2} e^{-t^\alpha} dt = \frac{\Gamma(\frac{2n+3}{\alpha})}{\pi \alpha (2n+2)!} r^{2n+2}.$$

Similarly, for  $\ell \in \mathbb{N}$  we can differentiate the first integral in (A.1) with respect to  $r$  to get

$$(A.2) \quad \frac{\partial^\ell}{\partial r^\ell} f(r; \alpha) = \frac{(-1)^{\lceil \frac{\ell}{2} \rceil}}{\pi \alpha} \sum_{k=0}^n \frac{(-1)^k \Gamma(\frac{2k+1+2\lceil \frac{\ell}{2} \rceil}{\alpha})}{(2k+o(\ell))!} r^{2k+o(\ell)} + \mathcal{R}(r; \alpha),$$

where  $o(\ell) = 1$  if  $\ell$  is odd and  $o(\ell) = 0$  otherwise, and

$$|\mathcal{R}(r; \alpha)| \leq \frac{\Gamma(\frac{2n+3+2\lceil \frac{\ell}{2} \rceil}{\alpha})}{\pi \alpha (2n+2+o(\ell))!} r^{2n+2+o(\ell)}.$$

For partial derivatives with respect to  $\alpha$ , we can use the decomposition (A.2) for  $\ell_1 \in \mathbb{N}_0$ ,  $\ell_2 \in \mathbb{N}$  and  $\ell := \ell_1 + \ell_2 \in \mathbb{N}$  to get a decomposition of the form

$$(A.3) \quad \frac{\partial^\ell}{\partial r^{\ell_1} \partial \alpha^{\ell_2}} f(r; \alpha) = \frac{(-1)^{\lceil \frac{\ell_1}{2} \rceil}}{\pi} \sum_{k=0}^n \frac{(-1)^k}{(2k + o(\ell_1))!} \frac{\partial^{\ell_2}}{\partial \alpha^{\ell_2}} \left[ \frac{\Gamma(\frac{2k+1+2\lceil \frac{\ell_1}{2} \rceil}{\alpha})}{\alpha} \right] r^{2k+o(\ell_1)} + \mathcal{R}(r; \alpha).$$

Here the partial derivatives in the summands can be computed explicitly in terms of polygamma functions, and the remainder term can be estimated as

$$(A.4) \quad |\mathcal{R}(r; \alpha)| \leq \frac{r^{2n+2+o(\ell_1)}}{\pi \alpha^{\ell_2+1} (2n+2+o(\ell_1))!} \int_0^\infty |\log(t)|^{\ell_2} t^{\frac{2n+3+2\lceil \frac{\ell_1}{2} \rceil}{\alpha}-1} |p_{\ell_2}(t)| e^{-t} dt,$$

where  $p_{\ell_2}$  stands for the polynomial of degree  $\ell_2$  given by

$$\frac{\partial^{\ell_2}}{\partial \alpha^{\ell_2}} [e^{-t^\alpha}] = \log(t)^{\ell_2} p_{\ell_2}(t^\alpha) e^{-t^\alpha},$$

(and  $p_0 \equiv 1$ ). Generally this integral cannot be evaluated exactly, but for given values of the parameters it can be estimated numerically rather efficiently, since the integrand is neither oscillating nor overly peaked.

#### UNIVARIATE BOUNDS FOR $r \rightarrow \infty$

As in [8], the latter integral in (A.1) can be rotated from the positive real axis to the line  $\{\tau e^{i\varphi} : \tau > 0\}$  for an arbitrary  $\varphi \in (-\frac{\pi}{\max(2\alpha, 1)}, 0)$ , resulting in

$$(A.5) \quad f(r; \alpha) = \frac{1}{\pi} \Re \left\{ e^{i\varphi} \int_0^\infty e^{e^{i\beta_2} r \tau} e^{e^{i\beta_1} \tau^\alpha} d\tau \right\},$$

where  $\beta_1 := \beta_1(\alpha) := \pi + \alpha\varphi \in (\frac{\pi}{2}, \pi)$  and  $\beta_2 := \frac{3\pi}{2} + \varphi \in (\frac{\pi}{2}, \frac{3\pi}{2})$ . Expanding the term  $e^{e^{i\beta_1} \tau^\alpha}$  and performing some elementary calculations for the summands yields

$$(A.6) \quad f(r; \alpha) = \sum_{k=1}^n \frac{(-1)^{k+1} \Gamma(k\alpha + 1) \sin(\frac{k\alpha\pi}{2})}{\pi k!} r^{-k\alpha-1} + \underbrace{\frac{1}{\pi} \Re \left\{ e^{i(\varphi+(n+1)\beta_1)} \int_0^\infty \tau^{(n+1)\alpha} M_{n+1}(e^{i\beta_1} \tau^\alpha) e^{e^{i\beta_2} r \tau} d\tau \right\}}_{=: \mathcal{R}(r; \alpha)},$$

for all  $n \in \mathbb{N}$ , where  $M_{n+1}$  is (the analytic continuation of) the function  $z \mapsto (e^z - \sum_{k=0}^n \frac{z^k}{k!})/z^{n+1}$ . Writing  $M_0(z) = e^z$  for notational convenience, the above expansion also holds for  $n \in \{-1, 0\}$ , with the understanding that the sum is zero in this case.

The functions  $M_k$  above satisfy the bound  $|M_k(z)| \leq \frac{1}{k!}$  for  $z$  with negative real part, as can be easily verified for  $k = 0$  and consequently proved inductively using the recursive formula  $\frac{d}{dz}[z^k M_k(z)] = z^{k-1} M_{k-1}(z)$  for  $k \geq 1$ . Since the term  $e^{i\beta_1} \tau^\alpha$  in the integral in (A.6) has a negative real part, the error term can thus be estimated by

$$|\mathcal{R}(r; \alpha)| \leq \frac{1}{\pi(n+1)!} \int_0^\infty \tau^{(n+1)\alpha} e^{\sin(\varphi)r\tau} d\tau = \frac{\Gamma((n+1)\alpha + 1)}{\pi(n+1)! |\sin(\varphi)|^{(n+1)\alpha+1}} r^{-(n+1)\alpha-1},$$

and since the true value of  $\mathcal{R}$  does not actually depend on the auxiliary parameter  $\varphi \in (-\frac{\pi}{\max(2\alpha, 1)}, 0)$ , the above estimate can be improved to

$$(A.7) \quad |\mathcal{R}(r; \alpha)| \leq \frac{\Gamma((n+1)\alpha + 1)}{\pi(n+1)! \sin(\pi_\alpha)^{(n+1)\alpha+1}} r^{-(n+1)\alpha-1},$$

where  $\pi_\alpha := \frac{\pi}{2 \max(\alpha, 1)}$ .



Differentiating (A.6) termwise with respect to  $r$ , we have

$$(A.8) \quad \frac{\partial^\ell}{\partial r^\ell} f(r; \alpha) = \frac{(-1)^\ell}{\pi} \sum_{k=1}^n \frac{(-1)^{k+1}}{k!} \frac{\Gamma(k\alpha + \ell + 1) \sin(\frac{k\alpha\pi}{2})}{r^{k\alpha + \ell + 1}} + \mathcal{R}(r; \alpha),$$

with

$$(A.9) \quad |\mathcal{R}(r; \alpha)| \leq \frac{\Gamma((n+1)\alpha + \ell + 1)}{\pi(n+1)! \sin(\pi_\alpha)^{(n+1)\alpha + \ell + 1}} r^{-(n+1)\alpha - \ell - 1}.$$

Finally, for pure and mixed partial derivatives with respect to  $\alpha$ , we may use the previous expansion as a stepping stone to obtain

$$(A.10) \quad \frac{\partial^\ell}{\partial r^{\ell_1} \partial \alpha^{\ell_2}} f(r; \alpha) = \frac{(-1)^{\ell_1}}{\pi} \sum_{k=1}^n \frac{(-1)^{k+1}}{k!} \frac{\partial^{\ell_2}}{\partial \alpha^{\ell_2}} \left[ \frac{\Gamma(k\alpha + \ell_1 + 1) \sin(\frac{k\alpha\pi}{2})}{r^{k\alpha + \ell_1 + 1}} \right] + \mathcal{R}(r; \alpha),$$

with

$$(A.11) \quad |\mathcal{R}(r; \alpha)| \leq \frac{1}{\pi} \int_0^\infty \tau^{\ell_1} \left| \frac{\partial^{\ell_2}}{\partial \alpha^{\ell_2}} \left[ e^{i(n+1)\beta_1 \tau^{(n+1)\alpha}} M_{n+1}(e^{i\beta_1 \tau^\alpha}) \right] \right| e^{\sin(\varphi)r\tau} d\tau.$$

In (A.10), the derivatives in the summands can again be computed in terms of the polygamma functions if necessary. In (A.11), the partial derivatives can be estimated in terms of the functions  $M_k$  introduced above by iterating the recursive formula  $M'_k = M_k - kM_{k+1}$ . The integral in (A.11) will be of the order  $\mathcal{O}(r^{-(n+1)\alpha - \ell_1 - 1} \log(r)^{\ell_2})$  for large values of  $r$ , and one can a posteriori take  $\varphi \rightarrow -\pi_\alpha$  since again the true value of  $\mathcal{R}(r; \alpha)$  does not depend on  $\varphi$ .

#### BIVARIATE BOUNDS FOR $r \rightarrow 0$

A random two-dimensional vector  $\mathbf{X}$  obeying a symmetric and *spherically contoured* bivariate stable distribution with stability index  $\alpha \in (0, 2)$  can be described in terms of its characteristic function:

$$\mathbb{E}[\exp(it^\top \mathbf{X})] = \exp(-|\mathbf{X}|^\alpha), \quad \mathbf{t} \in \mathbb{R}^2,$$

where  $|\cdot|$  refers to the standard  $\ell^2$ -based Euclidean norm. We refer to e.g. [45] for a comprehensive account on such distributions.

The density function  $f_{\mathbf{X}}$  of  $\mathbf{X}$  can be expressed at  $\mathbf{x} \in \mathbb{R}^2$  by the inverse Fourier transform of the characteristic function above, resulting in

$$f_{\mathbf{X}}(\mathbf{x}; \alpha) = \frac{1}{2\pi} \int_0^\infty J_0(|\mathbf{x}|t) t e^{-t^\alpha} dt;$$

see e.g. [23]. Here  $J_\nu$  with  $\nu = 0$  stands for the Bessel function of the first kind, which can for  $\nu \in \mathbb{N}_0$  and  $z \in \mathbb{C}$  be expressed as

$$(A.12) \quad J_\nu(z) = \sum_{k=0}^{\infty} \frac{(-1)^k}{k!(k+\nu)!} \left(\frac{z}{2}\right)^{2k+\nu}.$$

In this section we are interested in estimating partial derivatives of the density function  $f_{\mathbf{X}}$  in terms of  $|\mathbf{x}|$  and  $\alpha$ . For this purpose, we write

$$(A.13) \quad f(r; \alpha) := \frac{1}{2\pi} \int_0^\infty J_0(rt) t e^{-t^\alpha} dt, \quad r \geq 0,$$

for the radial density function of  $\mathbf{X}$ .

By well-known integral representation formulas [4, Equation (4.9.11)], we have the uniform bounds  $\|J_\nu\|_{L^\infty(\mathbb{R})} \leq 1$  on the real line for all  $\nu \in \mathbb{N}_0$ , and by standard recurrence relations [4, Equation (4.6.6)] we thus have  $\|J_\nu^{(\ell)}\|_{L^\infty(\mathbb{R})} \leq 1$  for all

$\nu \in \mathbb{N}_0$  and derivatives  $J_\nu^{(\ell)}$  of  $J_\nu$ . Hence we may expand the function  $J_0$  in (A.13) to obtain

$$f(r; \alpha) = \frac{1}{2\pi\alpha} \sum_{k=0}^n \frac{(-1)^k \Gamma(\frac{2k+2}{\alpha})}{(2^k k!)^2} r^{2k} + \mathcal{R}(r; \alpha),$$

with

$$|\mathcal{R}(r; \alpha)| \leq \frac{\Gamma(\frac{2n+4}{\alpha})}{2\pi\alpha(2n+2)!} r^{2n+2}.$$

Similarly, differentiating (A.13) with respect to  $r$ , and (A.12) for  $\nu = 0$  with respect to  $z$ , yields

$$\begin{aligned} & \frac{\partial^\ell}{\partial r^\ell} f(r; \alpha) \\ &= \frac{(-1)^{\lceil \frac{\ell}{2} \rceil}}{2\pi\alpha} \sum_{k=0}^n \frac{(-1)^k \{ \prod_{i=1}^{\ell} (2k + o(\ell) + i) \} \Gamma(\frac{2k+2+2\lceil \frac{\ell}{2} \rceil}{\alpha})}{(2^{k+\lceil \frac{\ell}{2} \rceil} (k + \lceil \frac{\ell}{2} \rceil)!)^2} r^{2k+o(\ell)} + \mathcal{R}(r; \alpha), \end{aligned}$$

for all  $\ell \in \mathbb{N}$ , where

$$|\mathcal{R}(r; \alpha)| \leq \frac{\Gamma(\frac{2n+4+2\lceil \frac{\ell}{2} \rceil}{\alpha})}{2\pi\alpha(2n+2+o(\ell))!} r^{2n+2+o(\ell)}.$$

Subsequently

$$\begin{aligned} \frac{\partial^\ell}{\partial r^{\ell_1} \partial \alpha^{\ell_2}} f(r; \alpha) &= \frac{(-1)^{\lceil \frac{\ell_1}{2} \rceil}}{2\pi} \sum_{k=0}^n \frac{(-1)^k \{ \prod_{i=1}^{\ell_1} (2k + o(\ell_1) + i) \}}{(2^{k+\lceil \frac{\ell_1}{2} \rceil} (k + \lceil \frac{\ell_1}{2} \rceil)!)^2} \frac{\partial^{\ell_2}}{\partial \alpha^{\ell_2}} \left[ \frac{\Gamma(\frac{2k+2+2\lceil \frac{\ell_1}{2} \rceil}{\alpha})}{\alpha} \right] r^{2k+o(\ell_1)} \\ &\quad + \mathcal{R}(r; \alpha), \end{aligned}$$

for all  $\ell_1 \in \mathbb{N}_0$  and  $\ell_2 \in \mathbb{N}$ , where

$$|\mathcal{R}(r; \alpha)| \leq \frac{r^{2n+2+o(\ell_1)}}{2\pi\alpha^{\ell_2+1}(2n+2+o(\ell_1))!} \int_0^\infty |\log(t)|^{\ell_2} t^{\frac{2n+4+2\lceil \frac{\ell_1}{2} \rceil}{\alpha}-1} |p_{\ell_2}(t)| e^{-t} dt.$$

Here  $p_{\ell_2}$  stands for the polynomials introduced in (A.4) above. Again, the integrals appearing on the right-hand side well-behaved enough for numerical approximation; see the discussion following (A.4).

#### BIVARIATE BOUNDS FOR $r \rightarrow \infty$

Nolan [45] records an asymptotic expansion for the density function of the *amplitude distribution* of  $\mathbf{X}$  as  $r \rightarrow \infty$ , which for the radial density function (A.13) translates as

$$(A.14) \quad f(r; \alpha) = \frac{1}{\pi^2} \sum_{k=1}^n \frac{(-1)^{k+1} 2^{k\alpha} \Gamma(\frac{k\alpha+2}{2})^2 \sin(\frac{k\alpha\pi}{2})}{k!} r^{-k\alpha-2} + \mathcal{O}(r^{-(n+1)\alpha-2}),$$

for  $\alpha \in (0, 2)$ ,  $r > 0$  and  $n \in \mathbb{N}$ . This can be obtained by expressing  $\mathbf{X}$  as a sub-Gaussian vector with respect to a certain totally skewed univariate stable distribution, which admits a similar asymptotic series expansion as described in [8]. Below we will obtain (A.14) in an alternative way that allows us to quantitatively control the error term.

We may rewrite (A.13) as

$$(A.15) \quad f(r; \alpha) = \frac{1}{2\pi} \Re \left\{ \int_0^\infty H_0(rt) t e^{-t^\alpha} dt \right\},$$

where  $H_0: \mathbb{C} \setminus (-\infty, 0] \rightarrow \mathbb{C}$  stands for the so-called Hankel function of the first kind [4, Section 4.7], defined in terms of the Bessel functions of the first kind ( $J_0$ ) and second kind ( $Y_0$ ) by

$$H_0(z) = J_0(z) + iY_0(z).$$

The functions  $H_\nu$ ,  $\nu \in \mathbb{N}_0$ , can be defined similarly in terms of  $J_\nu$  and  $Y_\nu$ . By well-known recurrence relations and connection formulas [43, Sections 10.6 and 10.4], each derivative  $H_\nu^{(\ell)}$  can again be expressed as a linear combination of functions  $H_{\nu'}$  with  $(\nu - \ell)_+ \leq \nu' \leq \nu + \ell$ .

Following the contour integration procedure described in [8], we can then rotate the integral in (A.15) from the positive real axis to the line  $\{e^{i\varphi}\tau : \tau > 0\}$  for an arbitrary  $\varphi \in (0, \frac{\pi}{\max(2\alpha, 1)})$  to get

$$(A.16) \quad f(r; \alpha) = \frac{1}{2\pi} \Re \left\{ e^{2i\varphi} \int_0^\infty H_0(e^{i\varphi} r \tau) \tau e^{i\beta_1 \tau^\alpha} d\tau \right\},$$

where  $\beta_1 := \beta_1(\alpha) := \pi + \alpha\varphi$  is as in (A.5). More precisely, this contour integration and the associated limiting procedure is permitted because

$$(A.17) \quad |H_\nu(z)| \leq \begin{cases} c_{1,\nu} (|z|^{-\nu} + |\log(z)|) & \text{for } 0 < |z| \leq 1 \\ c_{2,\nu} |z|^{-\frac{1}{2}} e^{-\Im(z)} & \text{for } |z| \geq 1 \end{cases}$$

for all  $\nu \in \mathbb{N}_0$ , with certain constants  $c_{i,\nu}$  that we will not elaborate on; we refer to [4, Sections 4.5 and 4.8] for this and more comprehensive asymptotic expansions for Hankel functions.

Because of (A.17), we also expand the term  $e^{i\beta_1 \tau^\alpha}$  in (A.16) and integrate termwise to get

$$f(r; \alpha) = \frac{1}{2\pi} \sum_{k=0}^n \frac{1}{k!} \Re \left\{ e^{i(2\varphi+k\beta_1)} \int_0^\infty H_0(e^{i\varphi} r \tau) \tau^{k\alpha+1} d\tau \right\} r^{-k\alpha-2} + \mathcal{R}(r; \alpha).$$

If we can show that the remainder term above is of the order  $\mathcal{O}(r^{-(n+1)\alpha-2})$  as  $r \rightarrow \infty$ , it follows automatically from the uniqueness property of asymptotic expansions that the principal term coincides with the one in (A.14). To this end we recall the functions  $M_k$  from (A.6) and write

$$\mathcal{R}(r; \alpha) = \frac{1}{2\pi} \Re \left\{ e^{i(2\varphi+(n+1)\beta_1)} \int_0^\infty H_0(e^{i\varphi} r \tau) \tau^{(n+1)\alpha+1} M_{n+1}(e^{i\beta_1} \tau^\alpha) d\tau \right\},$$

and since the term  $e^{i\beta_1 \tau^\alpha}$  above has a negative real part by assumption, we may estimate

$$|\mathcal{R}(r; \alpha)| \leq \frac{1}{2\pi(n+1)!} \left( \int_0^\infty |H_0(e^{i\varphi} r \tau)| \tau^{(n+1)\alpha+1} d\tau \right) r^{-(n+1)\alpha-2}$$

which is of the desired form. In light of (A.17), we may further take  $\varphi \rightarrow \frac{\pi}{2\max(\alpha, 1)} = \pi_\alpha$  so that

$$(A.18) \quad |\mathcal{R}(r; \alpha)| \leq \frac{1}{2\pi(n+1)!} \left( \int_0^\infty |H_0(e^{i\pi_\alpha} r \tau)| \tau^{(n+1)\alpha+1} d\tau \right) r^{-(n+1)\alpha-2}.$$

Similarly,

$$\begin{aligned} \frac{\partial^\ell}{\partial r^\ell} f(r; \alpha) &= \frac{(-1)^\ell}{\pi^2} \sum_{k=1}^n \frac{(-1)^{k+1} 2^{k\alpha} \left\{ \prod_{i=2}^{\ell+1} (k\alpha + i) \right\} \Gamma\left(\frac{k\alpha+2}{2}\right)^2 \sin\left(\frac{k\alpha\pi}{2}\right)}{k!} r^{-k\alpha-\ell-2} \\ &\quad + \mathcal{R}(r; \alpha) \end{aligned}$$

with

$$|\mathcal{R}(r; \alpha)| \leq \frac{1}{2\pi(n+1)!} \left( \int_0^\infty |H_0^{(\ell)}(e^{i\pi_\alpha} r \tau)| \tau^{(n+1)\alpha+\ell+1} d\tau \right) r^{-(n+1)\alpha-\ell-2},$$

and further

$$\begin{aligned} & \frac{\partial^\ell}{\partial r^{\ell_1} \partial \alpha^{\ell_2}} f(r; \alpha) = \\ & \frac{(-1)^{\ell_1}}{\pi^2} \sum_{k=1}^n \frac{(-1)^{k+1}}{k!} \frac{\partial^{\ell_2}}{\partial \alpha^{\ell_2}} \left[ \frac{2^{k\alpha} \left\{ \prod_{i=2}^{\ell_1+1} (k\alpha + i) \right\} \Gamma\left(\frac{k\alpha+2}{2}\right)^2 \sin\left(\frac{k\alpha\pi}{2}\right)}{r^{k\alpha+\ell_1+2}} \right] + \mathcal{R}(r; \alpha), \end{aligned}$$

with

(A.19)

$$|\mathcal{R}(r; \alpha)| \leq \frac{1}{2\pi} \int_0^\infty |H_0^{(\ell_1)}(e^{i\varphi} r\tau)| \tau^{\ell_1+1} \left| \frac{\partial^{\ell_2}}{\partial \alpha^{\ell_2}} [e^{i(n+1)\beta_1} \tau^{(n+1)\alpha} M_{n+1}(e^{i\beta_1} \tau^\alpha)] \right| d\tau.$$

The latter integrand can again be estimated in terms of the functions  $M_k$ ; see (A.11) and the relevant discussion. One will then end up with integrals that are analytically untractable, but not outside the reach of numerical estimation.

#### UNIFORM AND OSCILLATORY BOUNDS FOR $0 \ll r \ll \infty$

Here we present rather crude uniform bounds, and some refinements based on oscillatory integral techniques, of  $|\frac{\partial^{\ell_1+\ell_2}}{\partial r^{\ell_1} \partial \alpha^{\ell_2}} f(r; \alpha)|$  for “moderate” values of  $r$ , where none of the asymptotic expansions discussed earlier come close to approximating the true function with e.g. 2–3 summands. The precise range of these “moderate” values of  $r$  of course depends on  $\alpha$  and the  $\ell_i$ ’s. We present these estimates only in the univariate case, since the bivariate case can be handled with minor adjustments.

First, from (A.1), we have

$$(A.20) \quad \frac{\partial^{\ell_1+\ell_2}}{\partial r^{\ell_1} \partial \alpha^{\ell_2}} f(r; \alpha) = \frac{1}{\pi} \int_0^\infty \cos^{(\ell_1)}(rt) \log(t)^{\ell_2} t^{\ell_1} p_{\ell_2}(t^\alpha) e^{-t^\alpha} dt,$$

where  $\cos^{(\ell_1)}$  stands for the  $\ell_1$ ’th derivative of the cosine function, and  $p_{\ell_2}$  stands for the polynomial introduced in (A.4). Thus, a simple application of the triangle inequality yields

$$\left| \frac{\partial^{\ell_1+\ell_2}}{\partial r^{\ell_1} \partial \alpha^{\ell_2}} f(r; \alpha) \right| \leq \frac{1}{\pi \alpha^{\ell_2+1}} \int_0^\infty |\log(t)|^{\ell_2} t^{\frac{\ell_1+1}{\alpha}-1} |p_{\ell_2}(t)| e^{-t} dt.$$

The latter integral is again usually intractable (although it can be expressed in terms of the standard gamma function if  $\ell_2 = 0$ ), but numerically estimable.

In case  $\ell_2 = 0$  and  $\ell_1 := \ell > 0$ , we can slightly refine (A.20) using the oscillatory integral technique of partial integration against a function that decays sufficiently fast as  $t \rightarrow 0^+$  and  $t \rightarrow \infty$ :

$$(A.21) \quad \left| \frac{\partial^\ell}{\partial r^\ell} f(r; \alpha) \right| = \frac{1}{\pi r} \left| \int_0^\infty \cos^{(\ell-1)}(rt) \frac{d}{dt} [t^\ell e^{-t^\alpha}] dt \right| \leq \frac{1}{rt} \int_0^\infty \left| \frac{d}{dt} [t^\ell e^{-t^\alpha}] \right| dt.$$

The derivative inside the last integral can be easily computed, and one arrives at an upper bound for the integral that can be expressed in terms of the gamma function.

Similarly, when  $\ell_1 = 0$  and  $\ell_2 := \ell > 0$ , we have

$$\left| \frac{\partial^\ell}{\partial \alpha^\ell} f(r; \alpha) \right| = \frac{1}{\pi r} \left| \int_0^\infty \sin(rt) \frac{d^{\ell+1}}{dt d\alpha^\ell} [e^{-t^\alpha}] dt \right| \leq \frac{1}{\pi r} \int_0^\infty \left| \frac{d^{\ell+1}}{dt d\alpha^\ell} [e^{-t^\alpha}] \right| dt.$$

Again, the derivatives inside the last integral can be computed, and after a suitable change of variables we arrive at an integral directly proportional to  $\alpha^{-\ell}$ , where the coefficient of  $\alpha^{-\ell}$  can be calculated numerically.

This approach could also in principle be used for mixed derivatives of  $f(r; \alpha)$ , and in (A.21) the partial integration trick could be applied  $\ell$  times instead of once. In both cases however the computations become very unwieldy, and thus we discard them.

## GRID APPROXIMATIONS

Recall from the main paper (Section 3.1) that one of our primary goals is to estimate

$$(A.22) \quad \sup_{0 < r < 30, 0.5 \leq \alpha \leq 1.9} \left| \frac{\partial^{\ell_1 + \ell_2}}{\partial r^{\ell_1} \partial \alpha^{\ell_2}} \log f(r; \alpha) \right|$$

for  $(\ell_1, \ell_2) \in \{(4, 0), (2, 2), (0, 4)\}$ . Recalling that e.g.

$$\begin{aligned} (\log f(r; \alpha))^{(4,0)} &= -6 \frac{f^{(1,0)}(r; \alpha)^4}{f(r; \alpha)^4} + 12 \frac{f^{(2,0)}(r; \alpha) f^{(1,0)}(r; \alpha)^2}{f(r; \alpha)^3} \\ &\quad - 4 \frac{f^{(3,0)}(r; \alpha) f^{(1,0)}(r; \alpha)}{f(r; \alpha)^2} - 3 \frac{f^{(2,0)}(r; \alpha)^2}{f(r; \alpha)^2} + \frac{f^{(4,0)}(r; \alpha)}{f(r; \alpha)}, \end{aligned}$$

and similarly for the other relevant partial derivatives, we may estimate the suprema in (A.22) by applying the triangle inequality on sums of the above sort, and by estimating

- (1) the absolute values of the partial derivatives  $f^{(\ell_1, \ell_2)}(r; \alpha)$  from above, relying on the pointwise estimates established in the previous sections, and
- (2)  $f(r; \alpha)$  itself from below.

In this section we will give an overview of a numerical procedure to estimate these functions in a manner that is applicable for estimating (A.22).

We start with a fixed grid of the  $(r, \alpha)$ -space, with density given by a parameter  $\Delta > 0$  such that

$$\frac{1.9 - 0.5}{\Delta} =: i^*, \quad \text{and} \quad \frac{30}{\Delta} =: j^*,$$

are positive integers. In our numerical simulations we have used  $\Delta := \frac{2}{10^3}$  in order to conserve computational resources, but other choices are possible as well.

Write then

$$Q_{i,j} := [(j-1)\Delta, j\Delta] \times [0.5 + (i-1)\Delta, 0.5 + i\Delta] \quad \text{for } i \in 1:i^* \text{ and } j \in 1:j^*,$$

so that

$$\bigcup_{i,j} Q_{i,j} = [0, 30] \times [0.5, 1.9],$$

and the interiors of the  $Q_{i,j}$ 's are pairwise disjoint. The idea is to numerically estimate  $f(r; \alpha)$  and its partial derivatives uniformly in these squares, of which there is a finite amount, and the uniform estimates will not be too far off from the pointwise estimates we obtained in the earlier sections if the parameter  $\Delta$  is sufficiently small.

To this direction, let us first discuss the estimates of the absolute values of the partial derivatives  $f^{(\ell_1, \ell_2)}(r; \alpha)$  for  $(r, \alpha) \in Q_{i,j}$ . Many of the pointwise estimates we have discussed above – for example (A.2), (A.3), (A.4), (A.6), (A.7), (A.8), (A.9), (A.10), (A.11) and the bivariate versions of these estimates – consist of terms that are monotonous with respect to both  $r$  and  $\alpha$  either directly, or after some simple additional upper estimates, such as applying the triangle inequality in the sums like the ones in (A.2) and (A.8), and considering the cases  $r < 1$  and  $r \geq 1$  separately for terms of the form  $r^{k\alpha + \ell + 1}$ .

Some additional care has to be taken for some of the more complicated terms appearing in the series expansions for the partial derivatives involving the variable  $\alpha$ , as well as the respective remainder terms. We explain this with examples pertaining to the univariate case, but everything here applies to the bivariate case as well with obvious modifications.

First, the derivatives with respect to  $\alpha$  appearing in the summands in (A.3) and (A.10) can with some effort be computed for  $\ell_2 \in \{1, 2\}$ , resulting terms involving

the gamma function itself and the so-called polygamma functions of orders 0 and 1, which we denote here by  $\psi(0, \cdot)$  and  $\psi(1, \cdot)$  respectively. The function  $\psi(1, \cdot)$  is strictly positive and decreasing on the entire positive real axis (see e.g. [4, Theorem 1.2.5]), which implies the functions  $|\psi(0, t)|$  and  $|\Gamma(t)|$  are decreasing for  $0 < t \leq t_0$  and increasing for  $t > t_0$ , where  $t_0 \approx 1.46$  is the positive zero of  $\psi(0, \cdot)$ , which has to be taken into account when estimating the derivatives involving  $\Gamma$ . For  $\ell_2 > 2$ , we use (A.3) and (A.10) only with  $n = -1$  and  $n = 0$  respectively, avoiding the need to estimate these derivatives at all.

Secondly, the integrals appearing in (A.4) and (A.11) depend on  $\alpha$  (the latter also on  $r$ ) in less than immediately obvious ways. For (A.4), we simply note that

$$(A.23) \quad t^{\frac{2n+3+2\lceil\frac{\ell_1}{2}\rceil}{\alpha}} \leq \max\left(t^{\frac{2n+3+2\lceil\frac{\ell_1}{2}\rceil}{\alpha_-}}, t^{\frac{2n+3+2\lceil\frac{\ell_1}{2}\rceil}{\alpha_+}}\right) \quad \forall t > 0,$$

if  $\alpha_- \leq \alpha \leq \alpha_+$ , so it suffices to numerically precompute

$$\int_0^\infty |\log(t)|^{\ell_2} \max\left(t^{\frac{2n+3+2\lceil\frac{\ell_1}{2}\rceil}{0.5+(i-1)\Delta}}, t^{\frac{2n+3+2\lceil\frac{\ell_1}{2}\rceil}{0.5+i\Delta}}\right) t^{-1} |p_{\ell_2}(t)| e^{-t} dt,$$

for  $\ell_2 \in 1:4$ ,  $\lceil\frac{\ell_1}{2}\rceil \in \{0, 1\}$  and  $i \in 1:i^*$ , and use each of these for in the respective square  $Q_{i,j}$ . For numerical integration, we use the Julia library `QuadGK.jl`.

Concerning integrals of the form (A.11), we recall that parameter  $\beta_1 = \pi + \alpha\varphi$  depends on  $\alpha$ , and note that it possible to write

$$(A.24) \quad \frac{\partial^{\ell_2}}{\partial \alpha^{\ell_2}} \left[ e^{i(n+1)\beta_1} \tau^{(n+1)\alpha} M_{n+1}(e^{i\beta_1} \tau^\alpha) \right] = \tau^{(n+1)\alpha} (\log(\tau) + i\varphi)^{\ell_2} \sum_{k=0}^{\ell_2} b_{n,k} \tau^{k\alpha} M^{(k)}(e^{i\beta_1} \tau^\alpha),$$

where the coefficients  $b_{n,k}$  depend on  $\alpha$  but their absolute values do not. For example, for  $\ell_2 = 2$ , the latter expression can be written as

$$\begin{aligned} & (e^{i\beta_1} \tau^\alpha)^{n+1} (\log(t) + i\varphi)^2 \left( (n+1)^2 M(e^{i\beta_1} \tau^\alpha) - (2n+3) e^{i\alpha\varphi} \tau^\alpha M'(e^{i\beta_1} \tau^\alpha) \right. \\ & \quad \left. + (e^{i\alpha\varphi} \tau^\alpha)^2 M''(e^{i\beta_1} \tau^\alpha) \right). \end{aligned}$$

The crux of all this is that by applying the triangle inequality to (A.24) and using simple uniform estimates for  $M$  and its derivatives (which is possible since  $e^{i\beta_1} \tau^\alpha$  by construction always has negative real part), the integral appearing in (A.11) can be decomposed as a linear combination of integrals of the form

$$\int_0^\infty |\log(\tau) + i\varphi|^{\ell_2} \tau^{k\alpha + \ell_1} e^{\sin(\varphi)r\tau} dt, \quad n+1 \leq k \leq n + \ell_2 + 1.$$

Making the substitution  $r\tau =: t$ , doing some elementary massaging for the resulting integrand, taking  $\varphi \rightarrow -\pi_\alpha$  and using a discretization estimate similar to (A.23), we again end up with a finite collection of integrals that can be precomputed.

The bivariate version of this estimate, (A.19), comes with the additional ingredient of the Hankel functions, which we use the Julia library `SpecialFunctions.jl` to compute.

All in all, we have described several different ways to bound

$$(A.25) \quad \sup_{(r,\alpha) \in Q_{i,j}} |f^{(\ell_1, \ell_2)}(r; \alpha)|,$$

and for each square  $Q_{i,j}$ , we may take the smallest out of these bounds as the ultimate bound (A.25).

It then remains to estimate

$$\inf_{(r,\alpha) \in Q_{i,j}} f(r; \alpha),$$

from below. For this purpose, we have first precomputed  $f(r; \alpha)$  at the corners of the  $Q_{i,j}$ 's using different numerical integration routines for different ranges of the parameters; see Section 3.1 of the main paper, where this is explained in the context of the spline approximation.

We then observe that  $f(r; \alpha)$  is for fixed  $\alpha$  a decreasing function of  $r > 0$ , both in the univariate and in the bivariate case. Thus, writing  $Q_{i,j} =: [r_{-,j}, r_{+,j}] \times [\alpha_{-,i}, \alpha_{+,i}]$ , we may use the fundamental theorem of calculus to obtain

$$\begin{aligned} \inf_{(r,\alpha) \in Q_{i,j}} f(r; \alpha) &= \inf_{\alpha \in [\alpha_{-,i}, \alpha_{+,i}]} f(r_{+,j}; \alpha) \\ &\geq \min(f(r_{+,j}; \alpha_{-,i}), f(r_{+,j}; \alpha_{+,i})) - \frac{\Delta}{2} \sup_{(r,\alpha) \in Q_{i,j}} |f^{(0,1)}(r; \alpha)|, \end{aligned}$$

where the latter can further be estimated using the bounds discussed in the context of (A.25). It turns out that with a small enough  $\Delta$ , such as  $\Delta = \frac{2}{10^3}$ , this yields a fair lower bound for a function like  $f(r; \alpha)$  which is otherwise very difficult to bound from below.

#### TAIL ERROR BOUNDS

Here we establish relative error bounds for the series decompositions (A.6) and (A.14), used in the main paper with  $n = 3$  and  $r > 30$ .

First, in the univariate case, we can rewrite (A.6) as

$$\begin{aligned} f(r; \alpha) &= \sum_{k=1}^3 \frac{(-1)^{k+1} \Gamma(k\alpha + 1) \sin(\frac{k\alpha\pi}{2})}{\pi k!} r^{-k\alpha-1} + \mathcal{R}_4(r; \alpha) \\ &=: \sum_{k=1}^3 c_k^{\mathcal{S}}(\alpha) r^{-k\alpha-1} + \mathcal{R}_4(r; \alpha) =: \mathcal{S}_3(r; \alpha) + \mathcal{R}_4(r; \alpha), \end{aligned}$$

with

$$|\mathcal{R}_4(r; \alpha)| \leq \frac{\Gamma(4\alpha + 1)}{24\pi \sin(\pi\alpha)^{4\alpha+1}} r^{-4\alpha-1} := c_4^{\mathcal{R}}(\alpha) r^{-4\alpha-1}.$$

Thus, for  $r \geq 30$ , we have the following estimates:

$$\begin{aligned} \left| 1 - \frac{f(r; \alpha)}{\mathcal{S}_3(r; \alpha)} \right| &= \left| \frac{\mathcal{R}_4(r; \alpha)}{\mathcal{S}_3(r; \alpha)} \right| \leq \frac{c_4^{\mathcal{R}}(\alpha) r^{-4\alpha-1}}{|c_1^{\mathcal{S}}(\alpha)| r^{-\alpha-1} - |c_2^{\mathcal{S}}(\alpha)| r^{-2\alpha-1} - |c_3^{\mathcal{S}}(\alpha)| r^{-3\alpha-1}} \\ &= \frac{c_4^{\mathcal{R}}(\alpha) r^{-3\alpha}}{|c_1^{\mathcal{S}}(\alpha)| - |c_2^{\mathcal{S}}(\alpha)| r^{-\alpha} - |c_3^{\mathcal{S}}(\alpha)| r^{-2\alpha}}, \end{aligned}$$

assuming these calculations are valid in the sense of the latter denominator being positive for  $r = 30$  – numerical considerations show that this is indeed the case. The rightmost quantity is then a decreasing function of  $r \geq 30$ , and we thus get a uniform error bound by investigating it with  $r = 30$ :

$$\sup_{r > 30, 0.5 \leq \alpha \leq 1.9} \left| 1 - \frac{f(r; \alpha)}{\mathcal{S}_3(r; \alpha)} \right| \leq 0.00096.$$

In the bivariate case, we may proceed similarly, this time with (A.14) for  $n = 3$  and bounding the remainder term with (A.18). We can estimate the integral in (A.18) using grid-based numerical upper bounds like in the previous section. We thus find

$$\sup_{r > 30, 0.5 \leq \alpha \leq 1.9} \left| 1 - \frac{f(r; \alpha)}{\mathcal{S}_3(r; \alpha)} \right| \leq 0.0016.$$



We may then use the logarithm function’s basic continuity properties near 1 to infer

$$\sup_{r>30, 0.5\leq\alpha\leq 1.9} |\log f(r; \alpha) - \log \mathcal{S}_3(r; \alpha)| \leq \begin{cases} 0.00097 & \text{(univariate case);} \\ 0.0017 & \text{(bivariate case).} \end{cases}$$

#### REFERENCES

- [1] Achim, A., Basarab, A., Tzagkarakis, G., Tsakalides, P., and Kouamé, D. “Reconstruction of Ultrasound RF Echoes Modeled as Stable Random Variables”. In: *IEEE Transactions On Computational Imaging* 1 (2015), pp. 86–95.
- [2] Alekseev, A. K., Navon, I. M., and Steward, J. L. “Comparison of advanced large-scale minimization algorithms for the solution of inverse ill-posed problems”. In: *Optimization Methods and Software* 24.1 (2009), pp. 63–87.
- [3] Ament, S. and O’Neil, M. “Accurate and efficient numerical calculation of stable densities via optimized quadrature and asymptotics”. In: *Statistics And Computing* 28 (2018).
- [4] Andrews, G. E., Askey, R., and Roy, R. *Special Functions*. Encyclopedia of Mathematics and its Applications. Cambridge University Press, 1999. DOI: [10.1017/CB09781107325937](https://doi.org/10.1017/CB09781107325937).
- [5] Arjas, A., Roininen, L., Sillanpää, M. J., and Hauptmann, A. “Blind Hierarchical Deconvolution”. In: *2020 IEEE 30th International Workshop on Machine Learning for Signal Processing (MLSP)*. 2020, pp. 1–6. DOI: [10.1109/MLSP49062.2020.9231822](https://doi.org/10.1109/MLSP49062.2020.9231822).
- [6] Belov, I. “On the computation of the probability density function of  $\alpha$ -stable distributions”. In: *Mathematical Modelling and Analysis* (2005).
- [7] Belovas, I., Sakalauskas, L., Starikovicius, V., and Sun, E. “Mixed-Stable Models: An Application to High-Frequency Financial Data”. In: *Entropy* 23 (2021), p. 739. DOI: [10.3390/e23060739](https://doi.org/10.3390/e23060739).
- [8] Bergström, H. “On some expansions of stable distribution functions”. In: *Arkiv för Matematik* 2.4 (1952), pp. 375–378.
- [9] Bolin, D. “Spatial Matérn fields driven by non-Gaussian noise.” In: *Scandinavian Journal of Statistics* 41.3 (2014), pp. 557–579.
- [10] Borak, S., Härdle, W., and Weron, R. *Stable Distributions*. Tech. rep. Berlin, Heidelberg, 2005, pp. 21–44. DOI: [10.1007/3-540-27395-6\\_1](https://doi.org/10.1007/3-540-27395-6_1).
- [11] Calluari, A., Alonso-Marroquin, K., and Harré, M. “Closed-form solutions for the Lévy-stable distribution”. In: *Physical Review E* (2018).
- [12] Carlson, R. and Hall, C. “Error bounds for bicubic spline interpolation”. In: *Journal Of Approximation Theory* 7 (1973), pp. 41–47.
- [13] Chada, N. K., Iglesias, M., Roininen, L., and Stuart, A. M. “Parameterizations for ensemble Kalman Inversion.” In: *Inverse Problems* 34.5 (2019).
- [14] Chada, N. K., Lasanen, S., and Roininen, L. “Posterior convergence analysis of  $\alpha$ -stable sheet.” 2019. arXiv: [1907.03086](https://arxiv.org/abs/1907.03086).
- [15] Chada, N. K., Schillings, C., and Weissmann, S. “On the incorporation of box-constraints for ensemble Kalman inversion.” In: *Foundations of Data Science* 4.1 (2019).
- [16] Chada, N. K., Stuart, A. M., and Tong, X. T. “Tikhinov regularization within ensemble Kalman inversion.” In: *SIAM Journal on Numerical Analysis* 55.2 (2019).
- [17] Condat, L. “Discrete Total Variation: New Definition and Minimization”. In: *SIAM Journal on Imaging Sciences* 10 (2017), pp. 1258–1290.

- [18] Crisanto-Neto, J., Luz, M., Raposo, P. E., and Viswanathan, G. “An efficient series approximation for the Lévy  $\alpha$ -stable symmetric distribution”. In: *Physics Letters A* 382 (2018).
- [19] Damianou, A. C. and Lawrence, N. D. “Deep Gaussian processes”. In: *AISTATS* (2013), pp. 207–215.
- [20] Dogo, E. M., Afolabi, O. J., Nwulu, N. I., Twala, B., and Aigbavboa, C. O. “A Comparative Analysis of Gradient Descent-Based Optimization Algorithms on Convolutional Neural Networks”. In: *2018 International Conference on Computational Techniques, Electronics and Mechanical Systems (CTEMS)*. 2018, pp. 92–99.
- [21] Duffy, A. C. “An Introduction to Gradient Computation by the Discrete Adjoint Method”. Preprint at <http://computationalmathematics.org>. 2009.
- [22] Dunlop, M. M., Girolami, M. A., Stuart, A. M., and Teckentrup, A. “How deep are deep Gaussian processes?” In: *Journal of Machine Learning Research* 19.54 (2018), pp. 1–46.
- [23] E., K. E. and J., Z. “Modeling SAR images with a generalization of the rayleigh distribution”. In: *IEEE transactions on image processing* 13 (2004), 527–533. DOI: [10.1109/tip.2003.818017](https://doi.org/10.1109/tip.2003.818017).
- [24] Ge, X., Zhu, G., and Zhy, Y. “On the testing for alpha-stable distributions of network traffic”. In: *Computer Communications* 27 (2004), pp. 447–457.
- [25] Givoli, D. “A tutorial on the adjoint method for inverse problems”. In: *Computer Methods in Applied Mechanics and Engineering* 380 (2021), p. 113810.
- [26] Hall, C. A. and Meyer, W. W. “Optimal error bounds for cubic spline interpolation.” In: *Journal of Approximation Theory* 16.2 (1976), pp. 105–122.
- [27] Ibrahim, M. A. H. and Leong, W. “The Hybrid BFGS-CG Method in Solving Unconstrained Optimization Problems”. In: *Abstract and Applied Analysis* 2014 (2014), p. 6. DOI: [10.1155/2014/507102](https://doi.org/10.1155/2014/507102).
- [28] Kaipio, J. and Somersalo, E. *Statistical and computational inverse problems*. Springer-Verlag, 2004.
- [29] Kingma, D. P. and Ba, J. “Adam: A Method for Stochastic Optimization”. In: *3rd International Conference on Learning Representations, ICLR 2015, San Diego, CA, USA, May 7-9, 2015, Conference Track Proceedings*. 2015.
- [30] Kolokoltsov, V. N. *Markov Processes, Semigroups and Generators*. Berlin, New York: De Gruyter, 2011. ISBN: 9783110250114. DOI: [doi : 10 . 1515 / 9783110250114](https://doi.org/10.1515/9783110250114).
- [31] Kühn, F. *Lévy Matters VI: Lévy-Type Processes: Moments, Construction and Heat Kernel Estimates*. Lecture Notes in Mathematics. Springer International Publishing, 2017. ISBN: 9783319608877.
- [32] Lassas, M., Saksman, E., and Siltanen, S. “Discretization-invariant Bayesian inversion and Besov space priors”. In: *Inverse Problems & Imaging* 3.1 (2009), pp. 87–122.
- [33] Lassas, M. and Siltanen, S. “Can one use total variation prior for edge-preserving Bayesian inversion?” In: *Inverse Problems* 20.5 (2004), pp. 1537–1563. DOI: [10.1088/0266-5611/20/5/013](https://doi.org/10.1088/0266-5611/20/5/013).
- [34] Li, C., Dunlop, M., and Stadler, G. “Bayesian neural network priors for edge-preserving inversion”. In: *Inverse Problems and Imaging* (2022).
- [35] Lindgren, F., Rue, H., and Lindström, J. “An explicit link between Gaussian fields and Gaussian Markov random fields: the stochastic partial differential equation approach.” In: *J. R. Stat. Soc. Ser. B Stat. Methodol* 73 (2011), pp. 423–498.

- [36] Liu, D. and Nocedal, J. In: *Mathematical Programming* 45.1-3 (1989), pp. 503–528. ISSN: 0025-5610. DOI: [10.1007/BF01589116](https://doi.org/10.1007/BF01589116).
- [37] Mercan, S. and Alam, M. “Anomaly detection in hyperspectral imagery using Stable Distribution”. In: *Proceedings Of SPIE - The International Society For Optical Engineering* 8049 (2011).
- [38] Mittnik, S., Doganoglu, T., and Chenyao, D. “Computing the probability density function of the stable Paretian distribution”. In: *Mathematical And Computer Modelling* 29 (1999), pp. 235–240.
- [39] Mogensen, P. K. and Riseth, A. N. “Optim: A mathematical optimization package for Julia”. In: *Journal of Open Source Software* 3.24 (2018), p. 615. DOI: [10.21105/joss.00615](https://doi.org/10.21105/joss.00615).
- [40] Métivier, L., Brossier, R., Operto, S., and Virieux, J. “Full Waveform Inversion and the Truncated Newton Method”. In: *SIAM Journal on Scientific Computing* 35 (2013), B401–B437. DOI: [10.1137/120877854](https://doi.org/10.1137/120877854).
- [41] Neal, R. M. *Bayesian Learning for Neural Networks*. Springer-Verlag, 1996. ISBN: 0387947248.
- [42] Nikias, C. and Shao, M. *Signal processing with alpha-stable distributions and applications*. 1995.
- [43] *NIST Digital Library of Mathematical Functions*. <http://dlmf.nist.gov/>, Release 1.1.7 of 2022-10-15. F. W. J. Olver, A. B. Olde Daalhuis, D. W. Lozier, B. I. Schneider, R. F. Boisvert, C. W. Clark, B. R. Miller, B. V. Saunders, H. S. Cohl, and M. A. McClain, eds. URL: <http://dlmf.nist.gov/>.
- [44] Nolan, J. “An algorithm for evaluating stable densities in Zolotarev’s (M) parameterization”. In: *Mathematical And Computer Modelling* 29 (1999), pp. 229–233.
- [45] Nolan, J. “Multivariate elliptically contoured stable distributions: theory and estimation”. In: *Computational Statistics* 28 (2013), pp. 2067–2089.
- [46] Nolan, J. “Numerical calculation of stable densities and distribution functions”. In: *Communications In Statistics. Stochastic Models* 13 (1997), pp. 759–774.
- [47] Powell, M. J. D. “Some convergence properties of the conjugate gradient method”. In: *Mathematical Programming* 11.1 (1976), pp. 42–49.
- [48] Rasmussen, C. E. and Williams, C. K. I. *Gaussian Processes for Machine Learning*. Vol. 62. MIT Press, 2006.
- [49] Rodomanov, A. and Nesterov, Y. “Rates of superlinear convergence for classical quasi-Newton methods”. In: *Mathematical Programming* (2021).
- [50] Roininen, L., Huttunen, J. M. J., and Lasanen, S. “Whittle-Matérn priors for Bayesian statistical inversion with applications in electrical impedance tomography”. In: *Inverse problems and Imaging* 8 (2014).
- [51] Samorodnitsky, G. and Taqqu, M. S. *Stable non-Gaussian Random Processes*. Chapman & Hall, 1994.
- [52] Sato, K. *Lévy Processes and Infinitely Divisible Distributions*. Cambridge University Press, 1999.
- [53] Scherer, M., Rachev, S., Young, S., and Fabozzi, F. A. “FFT-based approximation of tempered stable and tempered infinitely divisible distributions”. Preprint at <https://statistik.econ.kit.edu/>. 2009.
- [54] Suuronen, J., Chada, N. K., and Roininen, L. “Cauchy Markov Random Field Priors for Bayesian Inversion”. In: *Statistics and Computing* 32 (2022), p. 33.
- [55] Suuronen, J., Emzir, M., Lasanen, S., Särkkä, S., and Roininen, L. “Enhancing industrial X-ray tomography by data-centric statistical methods.” In: *Data-Centric Engineering* 10 (2020).

- [56] Tarantola, A. *Inverse Problem Theory and Methods for Model Parameter Estimation*. Elsevier, 1987.
- [57] Teimouri, M. and Amindavar, H. “A Novel Approach to Calculate Stable Densities”. In: *Proceedings of the World Congress on Engineering 1* (2008).
- [58] Ye, N., Roosta-Khorasani, F., and Cui, T. “Optimization Methods for Inverse Problems”. In: *2017 MATRIX Annals*. Springer International Publishing, 2019, pp. 121–140. ISBN: 978-3-030-04161-8.
- [59] Zhao, Z., Emzir, M., and Särkkä, S. “Deep state-space Gaussian processes”. In: *Statistics and Computing* 31 (2021).
- [60] Zhu, C., Byrd, R. H., Lu, P., and Nocedal, J. “Algorithm 778: L-BFGS-B: Fortran Subroutines for Large-Scale Bound-Constrained Optimization”. In: 23.4 (1997), 550–560. ISSN: 0098-3500.

SCHOOL OF ENGINEERING SCIENCE, LAPPEENRANTA-LAHTI UNIVERSITY OF TECHNOLOGY, FI-53850, FINLAND

*Email address:* `jarkko.suuronen@lut.fi`

SCHOOL OF ENGINEERING SCIENCE, LAPPEENRANTA-LAHTI UNIVERSITY OF TECHNOLOGY, FI-53850, FINLAND

*Email address:* `tomas.soto@lut.fi`

DEPARTMENT OF ACTUARIAL MATHEMATICS AND STATISTICS, HERIOT WATT UNIVERSITY, EDINBURGH, EH14 4AS, UK

*Email address:* `neilchada123@gmail.com`

SCHOOL OF ENGINEERING SCIENCE, LAPPEENRANTA-LAHTI UNIVERSITY OF TECHNOLOGY, FI-53850, FINLAND

*Email address:* `lassi.roininen@lut.fi`